Chapter 4
Modeling the Fatigue Behavior of Fiber-Reinforced Composite Materials Under Constant Amplitude Loading

4.1 Introduction

The fatigue design of a structural component is based on the evaluation of the fatigue behavior of the constituent materials under loading conditions similar to those of the structural component that it will encounter during its operational life. The failure mechanisms of a fiber-reinforced composite material are more complex than those of a metallic one. A synergy of matrix cracks, layer delamination and finally fiber failure comprises the basic failure mechanisms of fiber-reinforced composite materials. Due to this complexity, the application of a simple theory for the quantification of the effect of each one of these failure mechanisms on the fatigue life of a composite material and the eventual establishment of a method for the derivation of design allowables is very difficult. On the other hand, the measurement of a number of macroscopic damage metrics that are affected by the development of the failure mechanisms is possible and requires only simple experimental procedures and set-ups. For example, the relationship between the applied load and the corresponding number of cycles up to failure, the remaining strength after a fatigue loading or the stiffness degradation during the application of a constant or variable amplitude loading pattern can be used for the derivation of reliable allowable values for the design of a structural component.

Significant research efforts have been devoted to the understanding of the fatigue behavior of fiber-reinforced composite materials and development of techniques to model the fatigue life and predict material behavior under different conditions. A large amount of fatigue data have been derived for composite materials under different loading patterns in several engineering domains, such as the aerospace and wind turbine industries, e.g., [1–5] during the last decades. Usually, the results are presented in terms of S–N curves (of any type), and the design allowables are defined based on the life of the examined material under specific applied loads. Depending on the nature and amount of available data, design allowables in terms of S–N curves can also be determined for any reliability

A. P. Vassilopoulos and T. Keller, *Fatigue of Fiber-reinforced Composites*,
Engineering Materials and Processes, DOI: 10.1007/978-1-84996-181-3_4,

level, taking into account the stochastic nature of the phenomenon, as described in Chap. 3 of this volume. The main drawback of this type of fatigue data interpretation is the necessity for the failure of the material in order to derive the S–N curve. This is based on destructive testing and there is no way to implement this method during fatigue loading to serve as a life-monitoring tool. A different damage metric must be used for this purpose. The behavior of this damage metric during fatigue life must be characterized with simple and limited experiments, without the need to reach material failure, so that the method can be used for estimation of the fatigue life of the examined material or structural component while it is in service.

A damage metric that fulfills these requirements is the stiffness of the material. Use of stiffness as a damage metric does not require the failure of the material since it can be measured in a non-destructive way. Moreover, as the stiffness of composite materials exhibits less scatter than strength, the modeling of the stiffness behavior during fatigue life can be performed based on fewer experimental data than those needed for a reliable statistical analysis of the fatigue behavior of the examined material based on the derived S–N curves. As it will be presented later on, the stiffness degradation measurements can be used for the derivation of S–N curves that do not correspond to failure, but to a stiffness degradation level. This kind of curve is very useful for the design of structures that comprises of moving parts, since it can constitute design allowables that conforms with specified limits of displacement (strains) in order to maintain the structure's geometry and avoid causing problems in operation either by conflicting movements between different parts or by undesirable changes in the aerodynamics of each structural component.

Regardless of the method used for modeling, the established model in terms of a mathematical expression can be used to interpolate or extrapolate the fatigue behavior for different numbers of fatigue cycles. However, the situation is not as simple for the modeling of the behavior of a composite material when it is loaded under different loading patterns, e.g., Tension-Tension (T-T), tension-compression (T-C) or Compression-Compression (C-C) fatigue. The effect of the different mean stress levels of the various loading cases is very critical for the fatigue life of any composite material. It is not easy to interpolate between different loading domains in order to model the behavior of the material under new loadings and the constant life diagrams (CLDs) were established to address this problem. Depending on the CLD formulation, the interpolation between known material behaviors can be linear or non-linear. However, the accuracy of a CLD can only be evaluated based on comparisons with available fatigue data for the examined material.

In this chapter, the types of S–N curves commonly used for composite materials are reviewed and a critical comparison of their modeling ability is made. The models based on the linear regression of the stress vs. the logarithm of the number of cycles to failure (Lin-Log) or the logarithm of the applied cyclic stress vs. the logarithms of the number of cycles to failure (Log–Log) is presented and their modeling accuracy is compared to the modeling accuracy of novel methods for the interpretation of fatigue data based on stochastic computational tools, such as artificial neural networks and genetic programming, as presented in [6–8].

The most commonly used constant life diagrams for composite materials and those most recently introduced are also presented in this chapter. Their predictive ability is evaluated by using the dataset in Chap. 2 and others from the literature. The applicability of the models, the need for experimental data and the accuracy of the predictions are considered as critical parameters for the evaluation.

The stiffness degradation during the fatigue life of the examined composite material was thoroughly examined in Chap. 2 as a function of several parameters: the loading case (C-C, T-T or T-C loading), the applied cyclic stress level and the percentage of fibers along the loading direction. A systematic statistical analysis, corresponding to a certain *R*-value and off-axis direction, proved that irrespective of the constant amplitude stress level, stiffness degradation data are satisfactorily fitted by standard statistical distributions. Modeling of the stiffness degradation can be used for the derivation of S–N curves that correspond to specific stiffness degradation levels and not to failure. Here, these stiffness-controlled curves, designated Sc-N curves, were determined for each *R*-ratio and off-axis direction and compared to fatigue strength curves. It is shown that these two kinds of curves can be correlated and it is thus possible to derive fatigue design allowables corresponding to specific levels of stiffness degradation and survival probability. Furthermore, even by using only half of the experimental data, Sc-N curves can still be accurately defined.

4.2 Which Type of S–N Curve?

One of the most explicit and straightforward ways to represent experimental fatigue data is the S–N diagram. It is preferred to other approaches for the modeling of the fatigue life of FRP composite materials, e.g., those based on stiffness degradation, or crack propagation measurements during lifetime, since it requires input data (applied load and corresponding cycles to failure) that can be collected using very simple recording devices.

Usually, fatigue data for preliminary design purposes are gathered in the region of fatigue cycles ranging between 10^3 and 10^7. However, depending on the application, high- or low-cycle fatigue regimes can be of interest. Additional data are needed in such cases to avoid the danger of poor modeling due to extrapolation in an unknown space. Although for the high-cycle fatigue regime long-term fatigue data must be acquired, the situation seems easier for low-cycle fatigue where static strength data can apparently be used in combination with the pure fatigue data. However, when the static strength data are considered in the analysis, other problems arise, and thus the use of quasi-static strength data for the derivation of fatigue curves (such as fatigue data for 1 or ¼ cycle) is arguable. No complete study on this subject exists. Previous publications, e.g., [9], showed that quasi-static data should not be a part of the S–N curve, especially when they have been acquired under strain rates much lower that those used in fatigue loading. The use of quasi-static data in the regression leads to incorrect slopes of the S–N curves as

presented in [9]. On the other hand, although excluding quasi-static data improved the description of the fatigue data, it introduced errors in the lifetime predictions when the low-cycle regime is important, as for example for loading spectra with a few high-load cycles.

The selection of the fatigue model that is established by fitting a mathematical equation to the experimental data is of paramount importance for any fatigue analysis. The fatigue model reflects the behavior of the experimental data to theoretical equations which are consequently used during design calculations. A number of different types of fatigue models (or types of S–N curves) have been presented in the literature, with the most "famous" being the empirical semi-logarithmic and logarithmic relationships. Based on these it is assumed that the logarithm of the loading cycles is linearly dependent on the cyclic stress parameter, or its logarithm. Fatigue models determined in this way do not take different stress ratios or frequencies into account, i.e., different model parameters should be determined for different loading conditions. Also, they do not take into account any of the failure mechanisms that develop during the failure process and these fatigue models therefore have the disadvantage of being case-sensitive, since they may derive very accurate modeling results for one material system under specified loading conditions but very poor results for another. Other more sophisticated fatigue formulations that also take the influence of stress ratio and/or frequency into account were also reported [10, 11]. A unified fatigue function that permits the representation of fatigue data under different loading conditions (different R-ratios) in a single two-parameter fatigue curve was proposed by Adam et al. [10]. In another work by Epaarachchi et al. [11], an empirical model that takes into account the influence of the stress ratio and loading frequency was presented and validated against experimental data from different glass fiber-reinforced plastic composites. Although these models seem promising, their empirical nature is a disadvantage as their predictive ability is strongly affected by the selection of a number of parameters that must be estimated or even, in some cases, assumed.

Methods for the S–N curve modeling of composite materials, also appropriate for the derivation of S–N curves that take into account the stochastic nature of the examined materials, have been established to permit the derivation of S–N curves with some statistical significance based on limited datasets e.g., [12, 13]. These statistical methods (already presented in detail in Chap. 3) are also based on a deterministic S–N equation for representation of the fatigue data; however a more complicated process, compared to the simple regression analysis, is followed for the estimation of model parameters. In addition, the methods introduce assumptions that also allow the run-outs (data from specimens that did not fail during loading) to be considered in the analysis.

Recently, artificial intelligence methods have been adopted for interpretation of the fatigue data of composite materials. Artificial intelligence methods have previously been used and validated in various fields. They appear to offer a means of dealing with many multivariate problems for which no exact analytical model exists or is very difficult to develop. Artificial neural networks (ANNs) have proved as very powerful tools for pattern recognition, data clustering, signal processing etc. During

the last 10 years, ANNs have been used to model the fatigue life of composite materials by modeling their S–N behavior, e.g. [14–17], or by deriving constant life diagrams in order to model the effect of different stress ratios on the fatigue life of an FRP composite system, see e.g., [18, 19]. They have also been used in other engineering problems, such as prediction of the multiaxial strength of composite materials, Lee et al. [20], or the modeling of the fatigue crack growth rate of bonded FRP-wood interfaces, Jia et al. [21]. A hybrid neuro-fuzzy method, designated ANFIS (Adaptive Neuro-Fuzzy Inference System), has been used to model the fatigue life of unidirectional and multidirectional composite laminates. Results of its application to two, different in general, material systems have been presented in [6, 22]. Finally, Genetic Programming (GP) has been successfully used as a tool for the derivation of S–N curves and modeling of the fatigue behavior of composite materials, as presented by Vassilopoulos et al. [8].

This innovative tool in the field of fatigue life modeling, based on genetic programming, is also introduced in this chapter and its ability to derive appropriate S–N curves is evaluated against traditional empirical and statistical methods. Selected experimental data from the database presented in Chap. 2 have been used for the application of the different models and comparison of their modeling ability. For the application of the GP method the GP software tool from RML Technologies, Inc., Discipulus™ [23] was used.

4.2.1 Empirical and Statistical S–N Formulations

As mentioned in Chap. 3, the easiest way to estimate the parameters of a fitted line representing material behavior is linear regression analysis, which can be performed even based on hand calculations. The resulting S–N curve yields an estimate of the mean time to failure as a function of the corresponding stress variable. In the S–N formulation, the stress variable σ can refer to any cyclic stress definition, $\sigma_{\max}$ (maximum cyclic stress), σ_a (cyclic stress amplitude) or even $\Delta\sigma$ (cyclic stress range). The mathematical expressions of the semi-logarithmic and logarithmic S–N formulations are given in Eqs. 4.1, 4.2:

$$\log(N) = A + B\sigma \; or \tag{4.1}$$

$$\sigma = \sigma_o N^{\left(-\frac{1}{k}\right)} \tag{4.2}$$

in which σ represents the selected stress variable and N the corresponding number of cycles to failure, while A, B, σ_0 and k are the model parameters that will be determined after the application of the process to the available fatigue data. The fatigue life is considered as the dependent variable whereas the stress or strain is considered as the independent variable for the fitting.

The appropriate formulations, Eq. 4.3, for Whitney's Weibull statistics, and Eq. 4.4 for the Sendeckyj's wear-out model were also used in this chapter for the

derivation of S–N curves, corresponding to a 50% reliability level (see Chap. 3 for definition of the model parameters).

$$\sigma_a = \sigma_o \left\{ [-\ln P_S(N)]^{\left(\frac{1}{\alpha_f k}\right)} \right\} (N)^{\left(-\frac{1}{k}\right)} \tag{4.3}$$

$$\sigma_{\max} = \beta \left[-\ln P_S(N)^{\frac{1}{\alpha_f}} \right] [(N - A)C]^{-G} \tag{4.4}$$

4.2.2 Genetic Programming for Fatigue Life Modeling

Genetic programming (GP) is a domain-independent problem-solving technique in which computer programs are evolved to solve, or approximately solve, problems. Genetic programming is a member of the broad family of techniques known as Evolutionary Algorithms. All these techniques are based on the Darwinian principle of reproduction and survival of the fittest and are similar to biological genetic operations such as crossover and mutation. Genetic programming addresses one of the central goals of computer science, namely automatic programming, which is to create, in an automated way, a computer program that enables a computer to solve a problem [24].

In genetic programming, the evolution operates on a population of computer programs of varying shapes and sizes. These programs are habitually represented as trees, as for example the one shown in Fig. 4.1, where the function $f(x) = 3r + ((x + 5) - 2y)$ is represented in tree format. The operations are performed in the "tree branches" and the result is given at the "tree root".

Genetic programming starts with an initial population of thousands or millions of randomly generated computer programs composed of random choices of the primitive functions and terminals as defined in the first and second preparatory steps (see below) and then applies the principles of biological evolution to create a new (and often improved) population of programs. This new population is

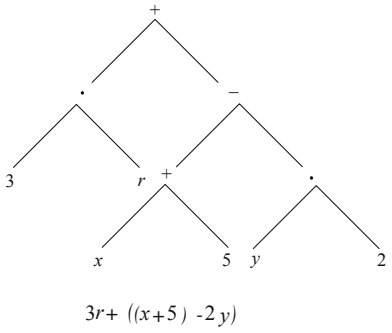

Fig. 4.1 Tree representation in genetic programming

generated in a domain-independent way using the Darwinian principle of survival of the fittest, an analogue of the naturally occurring genetic operation of crossover (sexual recombination), and occasional mutation [25]. The crossover operation is designed to create syntactically valid offspring programs (given closure amongst the set of programmatic ingredients). Genetic programming combines the expressive high-level symbolic representations of computer programs with the near-optimal efficiency of learning of Holland's genetic algorithm. A computer program that solves (or approximately solves) a given problem often emerges from this process [25].

Six major preparatory steps must be performed before applying genetic programming [25] in a given problem. These steps include preparation of datasets, setting-up of the model and design of the termination criteria, as explained in the following:

1. Determination of the *set of terminals*. The terminals can be seen as the inputs to the as-yet-undiscovered computer program. The set of terminals (or *Terminal Set T*, as it is often called) together with the set of functions is the ingredients from which genetic programming constructs a computer program to solve, or approximately solve, the problem.
2. Determination of the *set of primitive functions.* These functions will be used to generate the mathematical expression that attempts to fit the given finite sample of data. Each computer program is a combination of functions from the function set *F* and terminals from the terminal set *T*. The selected function and terminal sets should have the closure property in order that any possible combination of functions and terminals produces a valid executable computer program (a valid model).
3. Determination of the *fitness measure* which drives the evolutionary process. Each individual computer program in the population is executed and then evaluated, using the fitness measure, to determine how well it performs in the particular problem environment. The nature of the fitness measure varies with the problem: e.g., for many problems, fitness is naturally measured by the discrepancy between the result produced by an individual candidate program and the desired result; the closer this error is to zero, the better the program. For some problems, it may be appropriate to use a multi-objective fitness measure incorporating a combination of factors such as correctness, parsimony (smallness of the evolved program), and efficiency.
4. Determination of the *parameters for controlling the run*. These parameters define the guidelines in accordance with which each GP model that evolves. The population size, i.e., the number of created computer programs, the maximum number of runs, i.e., evolved program generations and the values of the various genetic operators are included in the list of parameters.
5. Determination of *the method for designating a result.* A frequently used method for result designation of a run is to appoint the best individual obtained in any generation of the population during the run, (i.e., the *best-so-far individual*) as being the result of the run.

6. Determination of *the criterion for terminating a run*. The maximum number of generations, or the maximum number of successive generations for which no improvement is achieved (values that were determined in step 4), is usually considered as the termination criteria.

Typically, the size of each developed program is limited, for practical reasons, to a certain maximum number of points (i.e., total number of functions and terminals) or a maximum depth of the program tree. Each computer program in the population is executed for a number of different *fitness cases* so that its fitness is measured as a sum or an average over a variety of different representative situations. For example, the fitness of an individual computer program in the population may be measured in terms of the sum of the absolute value of the differences between the output produced by the program and the correct answer (desired output) to the problem (i.e., the Minkowski distance) or the square root of the sum of the squares (i.e., Euclidean distance). These sums are selected from a sampling of different inputs (fitness cases) to the program. The fitness cases may be chosen at random or in a structured way (e.g., at regular intervals) [25].

All the individual programs of the initial population (generation 0) usually have exceedingly poor fitness, although some individuals in the population will fit the input data better than others. These differences in performance are then exploited by genetic programming. The Darwinian principle of reproduction and survival of the fittest and the genetic operations of crossover and mutation are used to create a new offspring population of individual computer programs from the current population.

The reproduction operation involves selecting a computer program from the current population of programs based on fitness (i.e., the better the fitness, the more likely the individual is to be selected) and allowing it to survive by copying it into the new population. Therefore, a new population, that of the offspring programs, replaces the old population. This iterative process is continued (new generations are evolved based on crossover and mutation operations) until a termination criterion, as defined in the sixth preparatory step, is satisfied. Regardless of their fitness, all generated programs, including those of the initial population, are syntactically valid executable programs.

The crossover operation creates new offspring computer programs from two parent programs selected on the basis of their fitness. The parent programs in genetic programming are usually of different shapes and sizes. The offspring programs are composed of sub-expressions from their parents. These offspring programs are usually of different shapes and sizes than their parents. For example, consider the two parent computer programs (models) represented as trees in Fig. 4.2 One crossover point is randomly and independently chosen in each parent. Consider that these crossover points are the division operator (/) in the first parent (the left one) and the multiplication operator (•) in the second parent (the right one). These two crossover fragments correspond to the underlying sub-programs (sub-trees) in the two parents–the sub-trees circled in Fig. 4.2. The two offspring resulting from the crossover operation, depicted in Fig. 4.3, have been created by

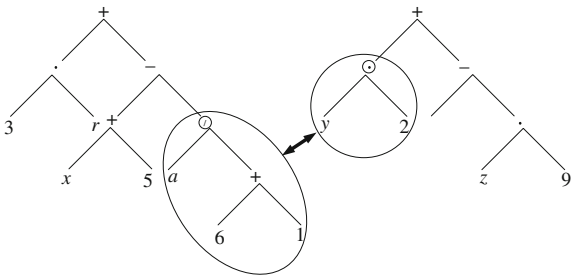

Fig. 4.2 Crossover operation: the two parent programs in tree representation

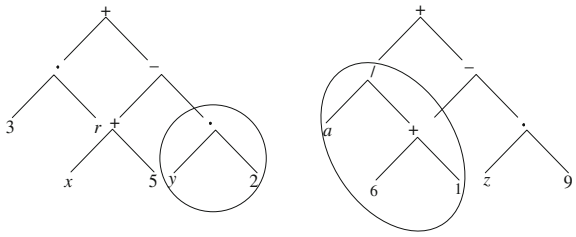

Fig. 4.3 Crossover operation: the two offspring programs in tree representation

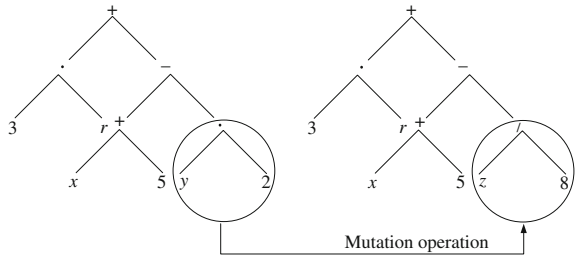

Fig. 4.4 Mutation operation of a parent program

swapping the two sub-trees between the two parents in Fig. 4.2. Thus, the crossover operation creates new computer programs using parts of existing parent programs. Since entire sub-trees are swapped, the crossover operation always produces syntactically and semantically valid programs as offspring, regardless of the choice of the two crossover points. Because programs are selected to participate in the crossover operation based on their fitness, crossover allocates future trials to regions of the search space whose programs contain parts from promising programs [25]. The crossover is the predominant operation in GP.

The mutation operation creates an offspring computer program from one parent program that is selected based on its fitness. One sub-tree is randomly and independently chosen and then substituted with another sub-tree, see Fig. 4.4, by using the same growth procedure as it was originally used to create the initial random population. There are several kinds of mutations possible. Some examples are [26] the branch-mutation, where a complete sub-tree is replaced by another, the node-mutation, which applies a random change to a single node, etc. This asexual mutation operation is typically performed sparingly during each generation.

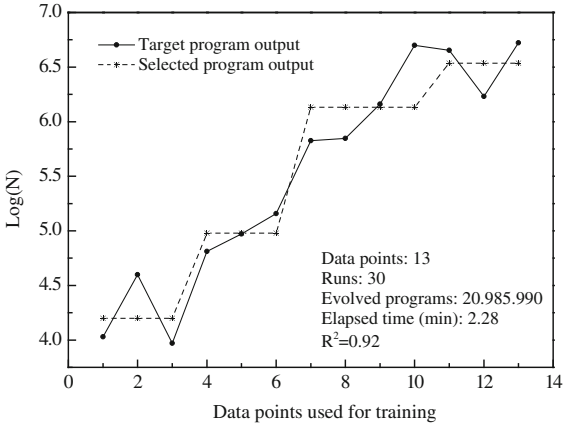

Fig. 4.5 Training of genetic programming model with experimental data for 0°, $R = -1$

The idea of modeling fatigue life with genetic programming was applied as described in the following:

The fatigue data of each dataset described in Chap. 2 was used for the training of the model and the selection of the best program.

- The training set contained the data which the tool used for learning. In other words, the fitness function was calculated based on the training set. Maximum stress values were used as the input parameters, while the corresponding cycles up to failure were considered as the desired output parameters. Given the number of input and output parameters in the training set, the process is characterized as a non-linear stochastic regression analysis.
- The validation set contained data for the evaluation of the evolved programs, after the training of the model, and the selection of the best one among them, based on the set criteria. In this case the criterion was the minimization of the error between the targeted output and the output produced by the evolved program. It is imperative that the validation set should contain examples that comprises of a good representative set of samples from the training domain.
- A test, or applied set, is constructed in the sequel, containing input data for which the output is expected to be calculated by the selected evolved program. Although these data are "new" and have not been used for the training or validation of the model, they should be in the range of the training set, since the ability of GP for extrapolation outside the training set has not yet been validated. For the case studied here, the test datasets were prepared so as to cover all the range from minimum to maximum cyclic stress levels in order to obtain, after the termination of each run, an entire S–N curve.

The same model (the selected evolved program) can be stored and potentially used to predict other output values for a new applied input dataset.

The training efficiency of the genetic programming tool was very good. As shown in Figs. 4.5, 4.6, 4.7, 4.8 where the target output is compared with the best program output after the training process for selected cases, the coefficient of

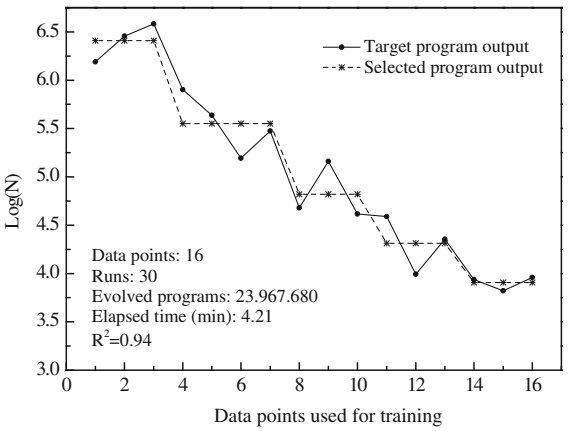

Fig. 4.6 Training of genetic programming model with experimental data for 15°, $R = 0.1$

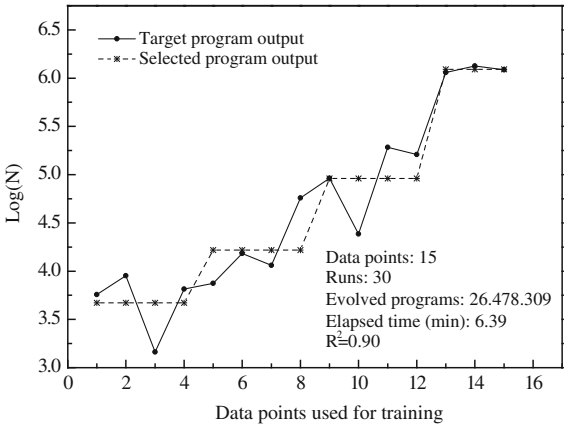

Fig. 4.7 Training of genetic programming model with experimental data for 45°, $R = 10$

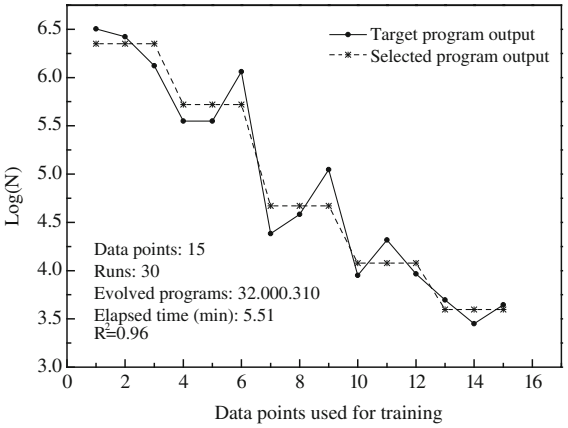

Fig. 4.8 Training of genetic programming model with experimental data for 75°, $R = 0.1$

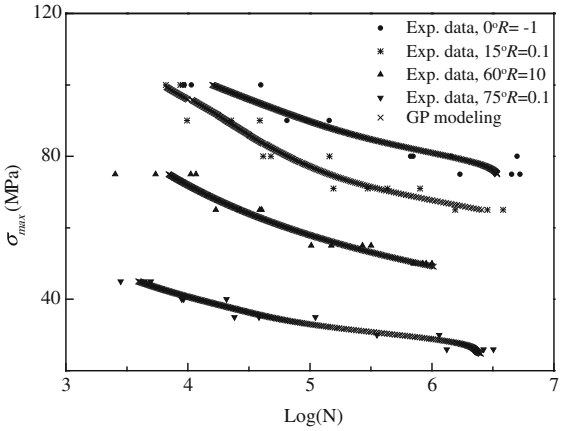

Fig. 4.9 Predicted S–N curves based on applied datasets and genetic programming

multiple determination (R^2), was in the range between 0.90 and 0.96. In the same Sures some information about running the GP model is also presented and can be described as follows:

- *Data points*: denote the number of data used for training the GP tool.
- *Runs*: The total number of evolving processes. During each run, new generations of the population are produced and usually evolve, i.e., the accuracy is improved. Each run finishes after 300 generations without improvement. It was decided to keep the number of runs constant for all examined cases.
- *Evolved programs*: The total number of computer programs that was evolved during the training process.
- *Elapsed time*: The total computer time required for the training of the model (depending on computer model).
- R^2: The coefficient of multiple determination, a statistical indicator that shows the accuracy of the model.

The GP tool was executed on an INTEL® Core™ i5 CPU 750 at 2.67 GHz, with 4 GB of RAM. As it can be seen in Figs. 4.5, 4.6, 4.7, 4.8 the data points used for each material case were preconditioned in different ways, sorted in ascending or descending order to prove the insensitivity of the proposed modeling technique to the treatment of the input data and also to avoid the generation of supervised modeling results.

After the development of a number of computer programs (during training) and the selection of the best one among them (during validation), the predictions (program output) were compared with the actual experimental data.

The results are presented in Fig. 4.9, where selected predicted S–N curves are plotted along with the experimental data for each material system on the S–N plane. As shown in Fig. 4.9, the modeling accuracy of genetic programming is excellent. In all the studied cases the produced curves follow the trend of the experimental data perfectly. It should be mentioned that the S–N curve predicted by the genetic programming tool is not of the predetermined type: power curve, or

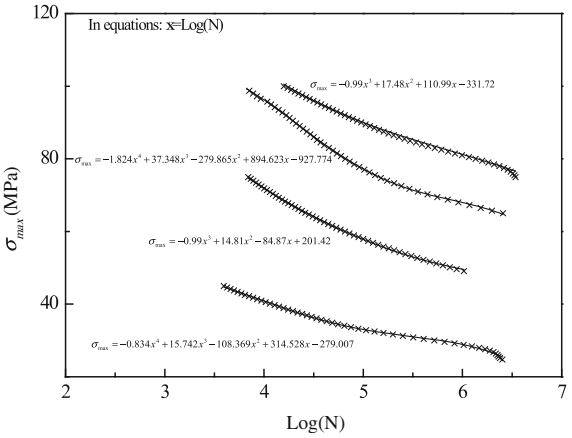

Fig. 4.10 Third and fourth order polynomial S–N curve equations for GP output

Table 4.1 Calculated fatigue model parameters for selected cases from the database presented in Chap. 2

	Linear regression, Eq. 4.2		Whitney, Eq. 4.3			Sendeckyj, Eq. 4.4			
Material	σ_o (MPa)	$1/k$	α_f	σ_o (MPa)	$1/k$	α_f	β (MPa)	G	C
0°, $R = -1$	164.31	−0.0517	1.51	155.71	−0.0463	29.37	105.10	−0.0476	1.54e−4
15°, $R = 0.1$	195.35	−0.0774	2.12	181.73	−0.0694	28.46	190.85	−0.0721	1.29
60°, $R = 10$	155.77	−0.0842	2.79	156.80	−0.0833	34.53	85.20	−0.0931	3.85e−4
75°, $R = 0.1$	88.63	−0.0838	2.06	83.82	−0.0769	26.31	86.73	−0.0781	1.44

polynomial, or semi-logarithmic etc. The resulting curve consists of data pairs (input and output) that can be simply plotted on the S–N plane. Using the model in this way suffices for the subsequent analysis, but output data, even if this is not necessary, can be easily fitted by a 2nd to 4th order polynomial equation, as shown in Fig. 4.10. Compared to Fig. 4.9, symbol frequency has been reduced and the scale of the x-axis has been extended to $\log(N) = 2$ in Fig. 4.10, but only for a better presentation of the research findings.

4.2.3 Comparison of the Modeling Ability of the S–N Curve Formulations

The fatigue data from Chap. 2 were analyzed using the selected methods and the fatigue model parameters were determined and, for cases arbitrarily selected from those examined, are tabulated in Table 4.1 After the determination of the fatigue model parameters, S–N curves can be easily derived for any range of loading cycles.

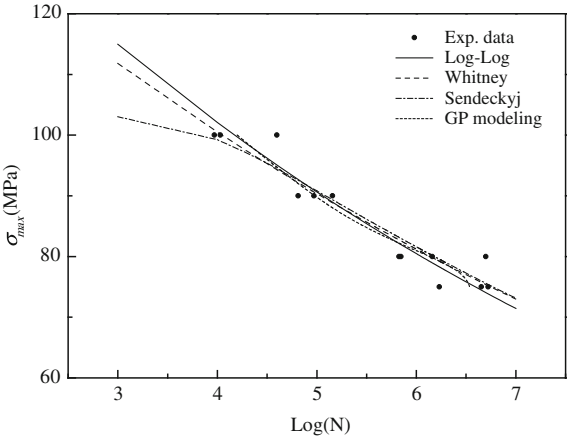

Fig. 4.11 Comparison of different fatigue modeling techniques, $R = -1$, $\theta = 0^o$

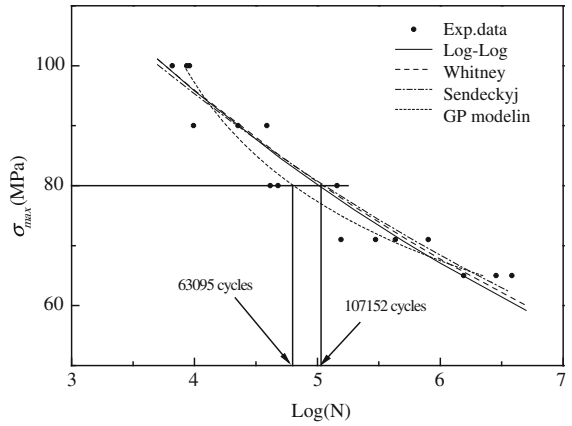

Fig. 4.12 Comparison of different fatigue modeling techniques, $R = 0.1$, $\theta = 15^o$

Fatigue behavior as modeled by all the available methods is presented in Figs. 4.11, 4.12, 4.13 and 4.14 for comparison. It can be concluded that although based on different approaches, in general all fatigue models could adequately represent the fatigue behavior of the selected experimental data, at least for the central part of the S–N curve, for $\log(N) = 3$ to $\log(N) = 6$. In all examined cases, Figs. 4.11, 4.12, 4.13 and 4.14 show that all fatigue models produce similar S–N curves with the Log–Log being steeper than the others. In some of the examined cases however, GP is shown to be superior as it can follow the real trend of the experimental data, without any constraints regarding a selected equation type. In Fig. 4.12, for example, where the predictions for the data obtained from specimens cut at 15° are presented, it is shown that the GP curve "follows" the trend of the experimental data more accurately than the other three fatigue models that result in a rather straight curve on the log(N)-S plane.

For example, when examining the stress level of 80 MPa, the experimental average number of cycles could be calculated as 77,985 and the corresponding

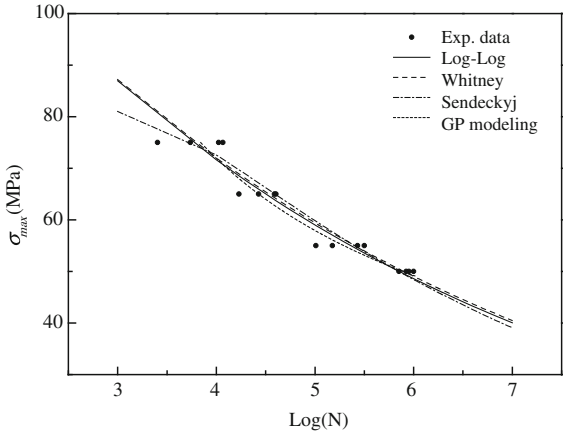

Fig. 4.13 Comparison of different fatigue modeling techniques, $R = 10$, $\theta = 60^o$

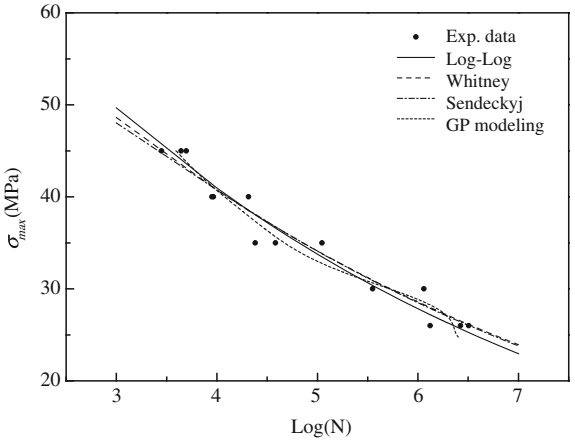

Fig. 4.14 Comparison of different fatigue modeling techniques, $R = 0.1$, $\theta = 75^o$

estimated numbers from the GP curve and other methods as 63,095 and 107,152 cycles, respectively. Moreover, for the stress level of 71 MPa, the GP tool estimates 380,189 loading cycles and the other methods approximately 562,341 loading cycles, while the experimental average is 421,213 loading cycles. For both examined stress levels, the GP curve underestimates the actual number of loading cycles by a factor of 9.7–19.1%, while the other curves overestimate the number of loading cycles by a factor of more than 33.5%. Although this conclusion is specific to the examined dataset, it shows the ability of the GP to adapt the model output to the given dataset.

The above comments were based on analysis of the available experimental fatigue data, without considering the corresponding static strengths of the examined material. Therefore, the validity of the modeling, without the need for extrapolation, is true only for numbers of cycles between ca 1,000 and 10 million.

4.2.4 Concluding Remarks

Several fatigue models for the derivation of S–N curves based on simple input fatigue data have been presented in order to evaluate their modeling ability and ascertain whether or not there is a type of S–N curve among those examined that exhibits superior features.

The results showed that for the range of cycles examined here (10^3–10^7) all examined models present similar accuracy. The simple deterministic formulation of Eq. 4.2, which resembles a pure mathematical fitting equation, is capable of modeling the fatigue life and can be used in preliminary design processes. However, a more detailed analysis of the results suggests that the statistical methods (e.g., those presented by Whitney and Sendeckyj) must be preferred when more accurate modeling is needed. The statistical methods take into account the fatigue data of specimens that did not fail during loading (run-outs) and are moreover based on assumptions regarding the relationship between static strength and fatigue data (wear-out model), which in a sense introduces into the process the mechanics of failure of the examined material. In addition they can be applied for the derivation of reliability-based S–N curves that can be very useful in the design of critical elements.

On the other hand, genetic programming has been proved to be a very powerful tool for modeling the non-linear behavior of composite laminates subjected to cyclic constant amplitude loading. It can be used to model the fatigue life of several composite material systems, and can be favorably compared with other modeling techniques. Here genetic programming has been used as a stochastic non-linear regression analysis tool. As the training dataset has been structured with a single input for a single output, the tool has been used to "fit" the behavior of the examined material. GP modeling is not based on any assumptions, as for example that the data follow a specific statistical distribution, or that the S–N curve is a power curve equation. Thus, the derived S–N curves do not follow any specific mathematical form but only the trend of the available data, giving each time the best estimate for their behavior. However, as shown here, the output data can be easily fitted by simple 3rd to 4th order polynomial equations. Although these facts alone suffice to justify the effectiveness of genetic programming as a modeling tool for the fatigue analysis of composite materials, the idea of using this tool for these types of analyses is not restricted to this application. The objective is to use more complex genetic programming configurations by introducing models with multiple inputs, e.g., stress amplitude, maximum stress, stress ratio and off-axis angle, and attempt to assign the corresponding number of cycles to failure to each set of inputs. It is anticipated that in such an analysis GP can be used as a predicting tool for several purposes, such as off-axis fatigue life prediction and construction of constant life diagrams .

Based on the above conclusions, all the examined S–N curve types are appropriate for modeling the fatigue life of composite materials. The empirical S–N formulations, like the one presented in Eq. 4.2, can be used for any

preliminary stage, since the model parameters can be estimated even by hand calculations. The more complicated numerical modeling represented here by the GP tool is useful when more a detailed description of fatigue behavior is required. The statistical methods Eqs. 4.3 and 4.4 are able to derive S–N curves for any desired reliability level and are therefore useful for design purposes where high reliability levels are desirable.

4.3 Constant Life Diagrams

A strong mean stress effect on the fatigue life of the on- and off-axis specimens was observed (see Chap. 2). The fatigue behavior of the examined material under different stress ratios was visualized in Chap. 2 by means of the constant life diagrams (see Figs. 2.11–2.13). In these figures, a linear interpolation between the known values was used, although, as will be shown in the following, this is not repeatedly the most appropriate method for composite materials.

In previous papers presented in the literature [27–32] it has been proved that, although the classic linear Goodman diagram is the most commonly used, particularly for metals, it is not suitable for composite materials, mainly because of the variation in the tensile and compressive strengths that they exhibit. The damage mechanisms under tension are different from those under compression. In tension, the composite material properties are generally governed by the fibers, while in compression the properties are mainly determined by the matrix and matrix-fiber interaction. Therefore, straight lines connecting the ultimate tensile stress (UTS) and the ultimate compressive stress (UCS) with points on the $R = -1$ line for different numbers of cycles are not capable of describing the actual fatigue behavior of composite materials. A typical constant life diagram (CLD) for composite materials is thus usually shifted to the right-hand side and the highest point located away from the line corresponding to zero mean stress, $\sigma_m = 0$.

Several CLD models have been presented in the literature [28–39] in order to deal with the aforementioned characteristics of composite materials. A comprehensive evaluation of the fatigue life predicting ability of the most commonly used and most recent is presented in [27]. Since the introduction of the constant life diagram concept by Gerber and Goodman back in the 19th century [40, 41], all presented methods have two common features–they represent the fatigue data on the (σ_m–σ_a)-plane and their formulation is based on the fitting of available fatigue data for specified R-ratios or the interpolation between them. The same concept has been followed for the derivation of CLDs for composite materials.

Starting from the basic idea of the symmetric and linear Goodman diagram and the non-linear Gerber equation, different modifications were proposed to cover the peculiarities of the behavior of composite materials. A linear model representing a modified Goodman diagram was presented in [42]. It is based on a single experimentally derived S–N curve and linear interpolation for the estimation of any others. More sophisticated models, although still based on the linear interpolation

between known S–N curve values and static strength data, were presented and analytical expressions for the theoretical derivation of any desired S–N curve were developed based on this idea [33, 43]. In the proposed models, a minimum of amount of experimental data was used, while simultaneously accommodating the particular characteristics of composites.

An alternative semi-empirical formulation was proposed in a series of papers by Harris's group [28, 29, 34]. The solution was based on fitting the entire set of experimental data with a non-linear equation to form a continuous bell-shaped line from the ultimate tensile stress to the ultimate compressive stress of the examined material. The drawback of this idea was the need to adjust a number of parameters based on experience and existing fatigue data. Kawai [30, 35] proposed the so-called anisomorphic CLD that can be derived by using only one "critical" S–N curve. The critical R-ratio is equal to the ratio of the ultimate compressive over the ultimate tensile stress of the examined material. The obvious drawback of this model is the need for experimental data for this specific S–N curve and therefore, theoretically, it cannot be applied to existing fatigue databases. However, the minimum amount of data required is an asset of the proposed methodology. Based on the Gerber line, another formulation of the CLD was proposed by Boerstra [36]. This offers a simple method for the lifetime prediction of laminated structures subjected to fatigue loads with continuously varying mean stress and dispenses with any classification of fatigue data according to R-values. The disadvantage of this method is the complicated optimization process with five variables that must be followed in order to derive the CLD model.

A new model was recently proposed by Kassapoglou [37, 38] based on the assumption that the probability of failure during any fatigue cycle is constant and equal to the probability of failure under static loading. Following this assumption, S–N curves under any loading pattern can be derived by using only tensile and compressive static strength data. However, the restricted use of static data disregards the different damage mechanisms that develops during fatigue loading and in many cases leads to erroneous results, e.g., [44].

A novel constant life diagram formulation was introduced in [39]. The model was established on the basis of the relationship between the stress ratio (R) and the stress amplitude (σ_a). Simple phenomenological equations were derived from this relationship without the need for any assumptions. The model parameters can be estimated based on a limited number of fatigue data. The validity of the proposed CLD formulation was evaluated by comparing predicted and experimental results for a wide range of composite materials. This new formulation, designated the "Piecewise Non-Linear model" (PNL), compares well with the existing ones, being more accurate in some of the studied cases for a wide range of glass and carbon fiber composite materials [39].

Novel computational methods have also been employed during the last decade for modeling the fatigue behavior of composite materials and the derivation of constant life diagrams based on limited amounts of experimental data, e.g., [8, 18, 19]. These methods offer a means of representing the fatigue behavior of the examined composite materials that is not biased by any damage mechanisms and not

restricted by any mathematical model description. They are data-driven techniques and their modeling quality depends on the quality of the available experimental data.

The influence of the constant life diagram formulation on the prediction of the fatigue life of composite materials was extensively studied in [27]. The most commonly used and most recent CLD formulations for composite materials are evaluated in this paragraph. The applicability of the models, the need for experimental data and the accuracy of their predictions are considered critical parameters for the evaluation. The effect of the selection of the CLD formulation on fatigue life prediction is assessed according to its ability to accurately estimate unknown S–N curves. The comparison of the modeling ability of the CLD formulations can also be based on the life prediction results of any life prediction methodology of which the CLDs are part. In this case however, other parameters that influence the results (i.e., other steps of the methodology concerning the selection of the S–N curve type for the data interpretation, damage summation rule, etc.) may mask the effect of the CLD formulation. Based on the results, recommendations concerning the applicability, advantages and disadvantages of each of the examined CLD formulations are discussed.

4.3.1 Theory of CLD Models

Constant life diagrams reflect the combined effect of mean stress and material anisotropy on the fatigue life of the examined composite material. Furthermore, they offer a predictive tool for the estimation of the fatigue life of the material under loading patterns for which no experimental data exist. The main parameters that define a CLD are the mean cyclic stress, σ_m, the cyclic stress amplitude, σ_a, and the R-ratio defined as the ratio between the minimum and maximum cyclic stress, $R = \sigma_{\min}/\sigma_{\max}$. A typical CLD annotation is presented in Fig. 4.15.

As shown, the positive (σ_m–σ_a)-half-plane is divided into three sectors, the central one comprising combined tensile and compressive loading. The Tension-Tension (T-T) sector is bounded by the radial lines, representing the S–N curves at $R = 1$ and $R = 0$, the former corresponding to static fatigue and the latter to tensile cycling with $\sigma_{\min} = 0$. S–N curves belonging to this sector have positive R-values less than unity. Similar comments regarding the two remaining sectors can be derived from the annotations shown in Fig. 4.15. Every radial line with $0 < R < 1$, i.e., in the T-T sector, has a corresponding symmetric line with respect to the σ_a-axis, which lies in the compression-compression (C-C) sector and whose R-value is the inverse of the tensile R-value, e.g., $R = 0.1$ and $R = 10$.

Radial lines emanating from the origin are expressed by:

$$\sigma_a = \left(\frac{1-R}{1+R}\right)\sigma_m \tag{4.5}$$

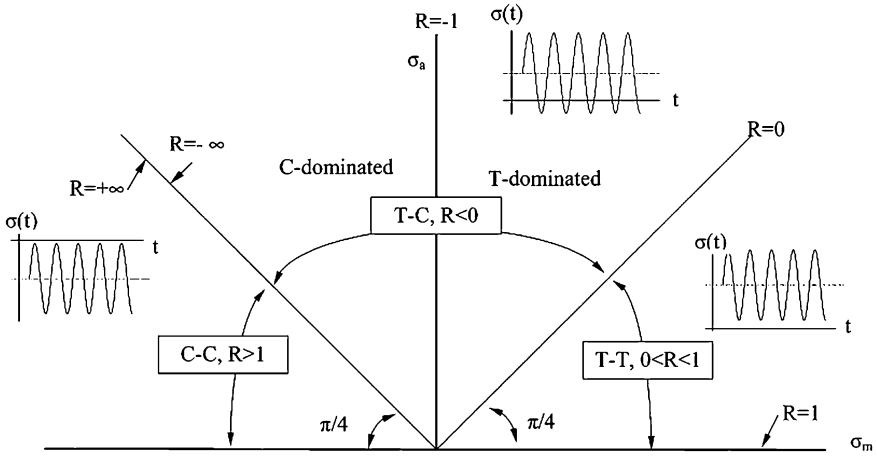

Fig. 4.15 Annotation for (σ_m–σ_a)-plane

and represent single S–N curves. Data on these lines belong to the S–N curve for that particular stress ratio. Constant life diagrams are formed by joining data points corresponding to the same numbers of cycles on consecutive radial lines.

Although from a theoretical point of view the above representation of the CLD is rational, it presents a deficiency, since it cannot accurately model the fatigue behavior of the examined material for loadings in the regions of the T-T (e.g., $R = 0.95$) and C-C (e.g., $R = 1.05$) sectors close to the horizontal axis, which represent loading under very low stress amplitude and high mean values with a culmination for zero stress amplitude ($R = 1$).

The classic CLD formulations require that the constant life lines converge to the ultimate tensile stress (UTS) and the ultimate compressive stress (UCS), regardless of the number of loading cycles. However, this is an arbitrary simplification originating from the lack of information about the fatigue behavior of the material when no amplitude is applied. In fact, this type of loading cannot be considered fatigue loading, but rather creep of the material (constant static load over a short or long period). Although modifications that take the time-dependent material strength into account have been introduced, their integration into CLD formulations requires the adoption of additional assumptions, see e.g., [32, 44].

4.3.1.1 Linear CLD

The concept of the linear CLD model [42] is based on a single S–N curve that must be experimentally derived. All other S–N curves can be determined from the given one by simple calculations. This simplified formulation assumes that the failure mechanism is identical in tension and in compression when the load amplitude is the same. In the (σ_m–σ_a)-plane, the above assumption implies that any constant life

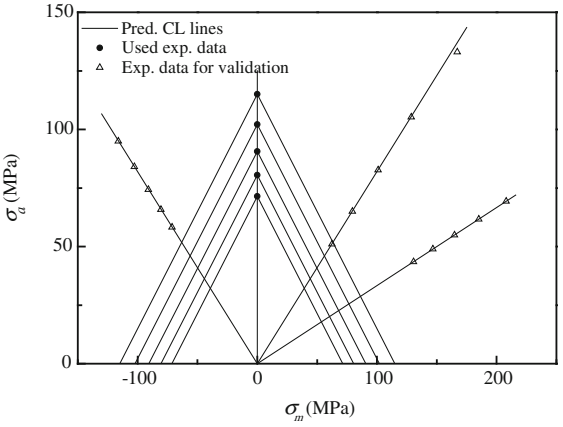

Fig. 4.16 Linear CLD for on-axis specimens, $N = 10^3$–10^7

line forms an isosceles triangle, subtending $\pi/4$ angles with the axes [42]. Any constant life line can be calculated by:

$$\frac{\sigma_a}{\sigma_o} + \frac{\sigma_m}{\sigma_o} = N^{-1/k} \tag{4.6}$$

where k and σ_0 are parameters of the power law equation which describes the S–N curve at the selected R-value.

The linear CLD for on-axis specimens of the examined material in Chap. 2 is presented in Fig. 4.16, based on the experimentally derived S–N curve under reversed loading.

4.3.1.2 Piecewise Linear CLD

The piecewise linear CLD [33, 43] is derived by linear interpolation between known values in the (σ_m–σ_a)-plane. This CLD model requires a limited number of experimentally determined S–N curves along with the ultimate tensile and compressive stresses of the materials. S–N curves representing the entire range of possible loading are commonly used for the construction of piecewise linear CLDs, normally at $R = 0.1$ for T-T loading, $R = -1$ for T-C loading and $R = 10$ for C-C loading patterns. Constant life lines connect data points of the same number of cycles on various S–N curves. Unknown S–N curves are calculated by linear interpolation between known values of fatigue and static strength data.

Analytical expressions were developed for the description of each region of the piecewise linear CLD in [43].

1. If R' is in the T-T sector of the CLD, and between $R = 1$ and the first known R-ratio on the (σ_m-σ_a)-plane when moving counterclockwise, R_{1TT}, then

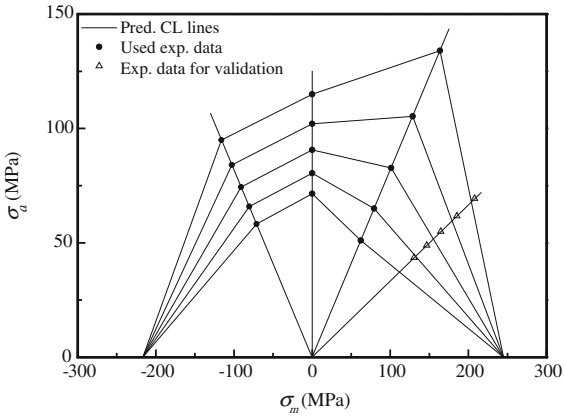

Fig. 4.17 Piecewise linear CLD for on–axis specimens, $N = 10^3$–10^7

$$\sigma'_a = \frac{UTS}{\frac{UTS}{\sigma_{a,1TT}} + r' - r_{1TT}} \tag{4.7}$$

in which σ'_a and $\sigma_{a,1TT}$ are the stress amplitudes corresponding to R' and R_{1TT}, respectively and $r_i = (1 + R_i)/(1 - R_i)$, and $r' = (1 + R')/(1 - R')$.

2. If R' is located between any of two known R-ratios, R_i and R_{i+1},

$$\sigma'_a = \frac{\sigma_{a,i}(r_i - r_{i+1})}{(r_i - r')\frac{\sigma_{a,i}}{\sigma_{a,i+1}} + (r' - r_{i+1})} \tag{4.8}$$

3. If R' lies in the C-C region of the CLD, and between $R = 1$ and the first known R-ratio in the compression region, R_{1CC},

$$\sigma'_a = \frac{UCS}{\frac{UCS}{\sigma_{a,1CC}} - r' + r_{1CC}} \tag{4.9}$$

where σ'_a and $\sigma_{a,1CC}$ are the stress amplitudes corresponding to R' and R_{1CC}, respectively.

The application of Eqs. 4.7–4.9 to the material data presented in Chap. 2 results in the CLD shown in Fig. 4.17 for the on-axis specimens.

4.3.1.3 Harris's CLD

Harris and his colleagues developed a semi-empirical equation based on fatigue test data obtained from a range of carbon and glass fiber composites [28, 29, 34]

$$a = f(1 - m)^u(c + m)^v \tag{4.10}$$

where a is the normalized stress amplitude component, σ_a/UTS, m the normalized mean stress component, σ_m/UTS, and c the normalized compression strength, UCS/UTS. In this equation, f, u and v are three adjustable parameters that are functions of fatigue life. The estimation of the parameters is based on the behavior of the material along the entire range of loading, combining T-T, C-C and T-C fatigue results. In this context, the formulation takes into account the combined effect of the different failure mechanisms that are developed under tension and under compression on the fatigue life. Early studies [28, 29] showed that parameter f mainly controls the height of the curve, and is a function of the ratio of the compressive to the tensile strength, while the exponents u and v determine the shapes of the two 'wings' of the bell-shaped curve. Initially, the model was established with two simplified forms of Eq. 4.10 where $u = v = 1$ and $u = v$ for a family of carbon/Kevlar unidirectional hybrid composites [28, 29]. Since this model was not accurate for different material systems,the general form of Harris's model was implemented in the sequel. In the general form, parameters f, u and v were considered as functions of fatigue life. Depending on the examined material, and the quality of the fatigue data, these parameters were found to depend linearly on the logarithm of fatigue life, $\log(N)$, for a wide range of FRP materials [29]:

$$f = A_1 \log(N) + B_1 \tag{4.11}$$

$$u = A_2 \log(N) + B_2 \tag{4.12}$$

$$v = A_3 \log(N) + B_3 \tag{4.13}$$

in which parameters A_i and B_i, $i = 1,2,3$, are determined by fitting Eqs. 4.11–4.13 to the available experimental data for different loading cycles.

Beheshty and Harris [29] showed that the selection of this empirical form for the parameters u and v can be employed for a wide range of materials, especially CFRP laminates. However, parameter f is sensitive to the examined material and its values vary considerably between GFRP and CFRP laminates. Since the modeling accuracy of the Harris CLD is significantly dependent on the quality of the fitting of these parameters, Harris and his colleagues established different formulations for the estimation of parameter f based on experimental evidence obtained from a number of different composite material systems. The most recent proposal for the estimation of parameter f is the following equation:

$$f = Ac^{-p} \tag{4.14}$$

where A and p are also functions of $\log(N)$. However, experimental evidence proved that values of $A = 0.71$ and $p = 1.05$ can be used in order to produce acceptable results for a wide range of CFRP and GFRP laminates [34].

The Harris CLD, also referred as the bell-shaped CLD, e.g., [42], looks like the one presented in Fig. 4.18 for the on-axis specimens of the materials of the

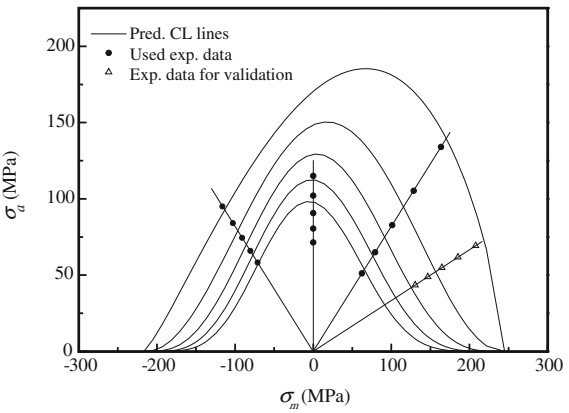

Fig. 4.18 Harris CLD for on-axis specimens, $N = 10^3$–10^7

examined dataset. Equation 4.14 with $A = 0.71$ and $p = 1.05$ was used for the derivation of parameter f. The other two parameters were estimated by fitting Eqs. 4.12–4.13 to the experimental data.

4.3.1.4 Kawai's CLD

Kawai's group [30, 35] developed a formula that describes an asymmetric constant life diagram, designated the anisomorphic constant fatigue life (CFL) diagram in [30]. The basic characteristic of this formulation is that it can be constructed by using only one experimentally derived S–N, designated the critical S–N curve. The R-ratio of this S–N curve is defined as the ratio of the ultimate compressive over the ultimate tensile stress of the examined material. The formulation is based on three main assumptions:

1. The stress amplitude, σ_a, for a given constant value of fatigue life N is greatest at the critical stress ratio,
2. The shape of the CFL curves changes progressively from a straight line to a parabola with increasing fatigue life, and
3. The diagram is bounded by the static failure envelope, i.e., two straight lines connecting the ultimate tensile and ultimate compressive stresses with the maximum σ_a on the critical S–N curve.

The CFL formulation depends on the position of the mean stress on the $(\sigma_m$–$\sigma_a)$-plane, whether it is in the tensile or compressive region. The mathematical formulation reads:

$$\frac{\sigma_a^{\chi} - \sigma_a}{\sigma_a^{\chi}} = \begin{cases} \left(\frac{\sigma_m - \sigma_m^{\chi}}{UTS - \sigma_m^{\chi}}\right)^{(2-\psi_x)}, & UTS \geq \sigma_m \geq \sigma_m^{\chi} \\ \left(\frac{\sigma_m - \sigma_m^{\chi}}{UCS - \sigma_m^{\chi}}\right)^{(2-\psi_x)}, & UCS \leq \sigma_m \leq \sigma_m^{\chi} \end{cases} \tag{4.15}$$

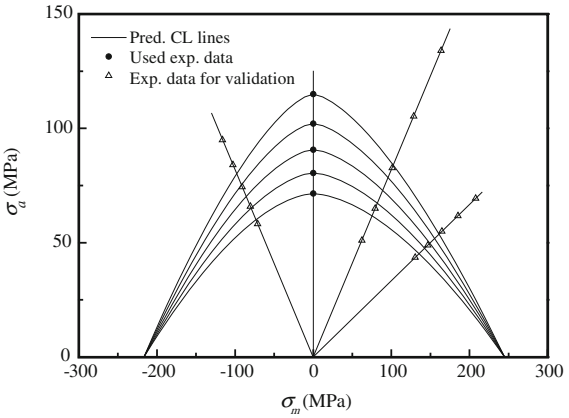

Fig. 4.19 Kawai's CLD for on-axis specimens, $N = 10^3$–10^7

where σ_m^{χ} and σ_a^{χ} represent the mean and cyclic stress amplitudes for a given constant value of life N under fatigue loading at the critical stress ratio. ψ_x denotes the critical fatigue strength ratio and is defined as:

$$\psi_{\chi} = \frac{\sigma_{\max}^{\chi}}{\sigma_B} \tag{4.16}$$

where $\sigma_{\max}^{\chi}$ is the maximum fatigue stress for a given constant value of life N under fatigue loading at the critical stress ratio. $\sigma_B(>0)$ is the reference strength (the absolute maximum between UTS and UCS) of the material that defines the peak of the static failure envelope. Therefore this normalization guarantees that ψ_x always varies in the range [0, 1] and the exponents $(2-\psi_x)$ in Eq. 4.15 are always greater than unity. Subsequently, linear (when $2-\psi_x = 1$) or parabolic (when $2-\psi_x > 1$) curves can be obtained from Eq. 4.15.

The critical fatigue strength ratio (see Eq. 4.16) is related to the number of loading cycles defining the normalized critical S–N curve:

$$\psi_{\chi} = f(2N_f) \tag{4.17}$$

After determining the critical S–N curve by fitting to the available fatigue data, the CFL diagram can be constructed on the basis of the static strengths, UTS and UCS, and the critical S–N relationship. The dependence of the anisomorphic CFL diagram on the critical S–N curve limits its applicability to the datasets for which available data under the critical R-ratio exist. When no-S-N curve under the critical R-ratio exists, the one that is closest to this value can be used as proposed in [27]. This was also the process followed for the derivation of the anisomorphic CFL diagram of the on-axis specimens of the examined dataset, which is presented in Fig. 4.19.

A modified anisomorphic CFL formulation was recently introduced by Kawai and Murata [45] to improve the performance of the original anisomorphic diagram. The authors observed that the fatigue behavior of matrix-dominated CFRP laminates cannot be described by simple linear or curved lines between the UTS, and the stress

amplitude of the critical S–N curve. Therefore they introduced the use of another S–N curve designated the "sub-critical" S–N curve in order to subdivide, wherever necessary, the sectors between the static strengths and the critical S–N curve, and eventually accurately fit the material behavior. The modified CFL diagram was proved accurate for modeling the fatigue behavior of the material investigated in [45] but its applicability is very limited to the examined material and cannot be generalized without additional experimental data.

4.3.1.5 Boerstra's CLD

Boerstra [36] proposed an alternative formulation for a CLD that can be applied to random fatigue data, which do not necessarily belong to an S–N curve. In this model, the *R*-ratio is not considered a parameter in the analysis and the model can be applied to describe the behavior of the examined material under loads with continuously changing mean and amplitude values. Boerstra's model constitutes a modification of the Gerber line. The exponent was replaced by a variable also including the difference in tension and compression. The general formulae of the model are:

$$\text{For } \sigma_m > 0: \quad \sigma_{ap} = \sigma_{Ap}\left(1 - \left(\sigma_m / UTS\right)^{\alpha T}\right) \tag{4.18}$$

$$\text{For } \sigma_m < 0: \quad \sigma_{ap} = \sigma_{Ap}\left(1 - \left(\sigma_m / UCS\right)^{\alpha C}\right) \tag{4.19}$$

where σ_{ap} is the stress amplitude component for a reference number of cycles, N_p, σ_{AP} is an "apex" stress amplitude for N_p and $\sigma_m = 0$, and αT and αC are two shape parameters of the CLD curves for the tensile and compressive sides, respectively.

The above equations represent the CLD lines in the (σ_m–σ_a)-plane. According to the author [35], existing fatigue data for different kinds of composite materials show steeper S–N curves under tension and than under compression. An exponential relationship with the mean stress can be a good description for the slope ($1/m$) of S–N lines as follows:

$$m = m_o e^{\left(-\sigma_m / D\right)} \tag{4.20}$$

in which m_o is a measure for the slope of the S–N curve on the Log–Log scale for $\sigma_m = 0$ and D is the skewness parameter for the dependency of m.

Equations 4.18–4.20 suggest that five parameters, m_o, D, N_p, αT, and αC, must be defined in order to construct the CLD model. However, the estimation of the parameters requires a multi-objective optimization process. The aim of this optimization is to estimate the parameters allowing the calculation of the shortest distance between each measuring point and the S–N line for its particular mean stress. The procedure is as follows:

1. The static strengths UTS and UCS are determined and some fatigue test data on specimens with various values of stress amplitude, σ_α, and mean stress, σ_m, should also be available.

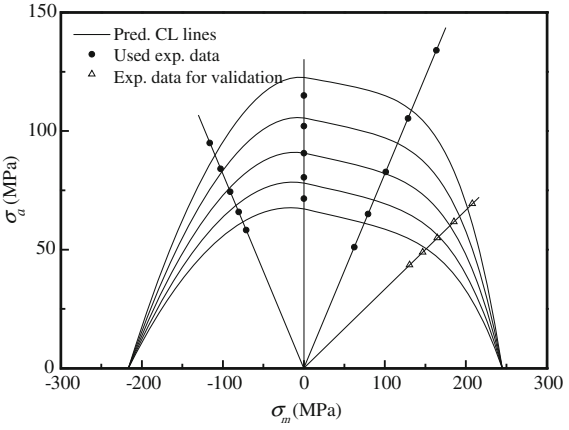

Fig. 4.20 Boerstra CLD for on-axis specimens, based on experimental data, $N = 10^3$–10^7

2. The desired value of N_p is chosen and an initial set of values for parameters m_o, D, N_p, αT and αC is assumed.
3. The slope of the S–N line, m, is calculated for each measured σ_m using Eq. 4.20.
4. The σ_α corresponding to each σ_m is projected to the (σ_m–σ_a)-plane for the selected number of cycles N_p by $\sigma_{ap} = \sigma_a(N/N_p)^{(1/m)}$.
5. $\sigma_{\alpha P}$ is calculated for each pair of σ_{0p} and σ_m using Eqs. 4.18 and 4.19.
6. A modified stress amplitude, $\sigma_{ap,mod}$, is calculated by feeding back the average value of σ_{AP} and the measured mean stress value, σ_m, into Eqs. 4.18 and 4.19.
7. The difference between the logarithms of the measured stress amplitude and the modified stress amplitude is then computed as: $\Delta\sigma_a = \ln(\sigma_{ap}) - \ln(\sigma_{ap,mod})$.
8. The theoretical number of cycles, N_e, corresponding to the $\sigma_{ap,mod}$ stress amplitude and the measured mean stress, σ_m, can be calculated by solving the equation:

$$N_e = N_p\left(\frac{\sigma_{a,\mathrm{mod}}}{\sigma_a}\right)^m \tag{4.21}$$

9. The difference between the measured number of cycles, N, and the theoretical number of cycles, N_e, is defined by $\Delta n = \ln(N) - \ln(N_e)$.
10. The shortest distance between each independent point and the S–N lines in the σ_m–σ_a-N space is expressed by: $\Delta t = sign(\Delta\sigma_a)\sqrt{(1/(1/\Delta\sigma_a^2 + 1/\Delta n^2))}$. The sum of all Δts is designated as the total standard deviation, SDt. Minimization of the SDt results in the estimation of the optimal m_o, D, N_p, αT and αC parameters.

The CLD that results from the above is presented in Fig. 4.20. The experimental fatigue data were directly considered in the analysis without the derivation

of any S–N curves. However, the process can be equally applied to fatigue data obtained by S–N curve equations, derived after fitting of the experimental data, as will be presented in the following.

4.3.1.6 Kassapoglou's CLD

A very simple model was recently proposed by Kassapoglou [37, 38]. Although proposed for the derivation of S–N curves under different R-ratios, this model can potentially be used for the construction of a piecewise non-linear CLD. The basic assumption of the model is that the probability of failure of the material during a cycle is constant and independent of the current state or number of cycles up to this point. This assumption oversimplifies the reality and masks the effect of the different damage mechanisms that develop under static loading and at different stages of fatigue loading. However, adoption of this assumption allows the estimation of the parameters of a single distribution based on the static strength data and use of this same distribution for the calculation of the fatigue life of the examined material. In this case, this model requires no fatigue testing, no empirically determined parameters and no detailed modeling of damage mechanisms.

The model comprises the following equations for calculation of maximum cyclic stress as a function of number of cycles:

$$\sigma_{\max} = \frac{\beta_T}{(N)^{\frac{1}{a_T}}}, \text{ for } 0 \le R < 1 \tag{4.22}$$

$$\sigma_{\max} = \frac{\beta_C}{(N)^{\frac{1}{a_C}}}, \text{ for } R > 1 \tag{4.23}$$

while for $R < 0$ the following equation should be solved numerically:

$$N = \frac{1}{\left(\frac{\sigma_{\max}}{\beta_T}\right)^{a_T} + \left(\frac{\sigma_{\min}}{\beta_C}\right)^{a_C}} \tag{4.24}$$

Parameters a_i, β_i, $i = T$ or C denote the scale and shape of a two-parameter Weibull distribution that can describe the static data in tension and compression respectively.

This model cannot be applied to the examined material described in Chap. 2 since the amount of available experimental static strength data is limited and therefore it is not possible to fit a reliable statistical distribution on them.

4.3.1.7 The Piecewise Non-Linear CLD

All previous CLD formulations are based on the fitting of linear or non-linear equations to existing fatigue data on the (σ_m–σ_a)-plane. However, there is no

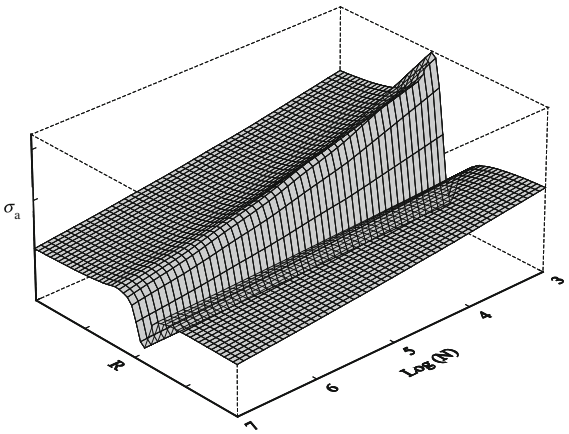

Fig. 4.21 Representation of relationship between fatigue parameters σ_a–R–Log(N)

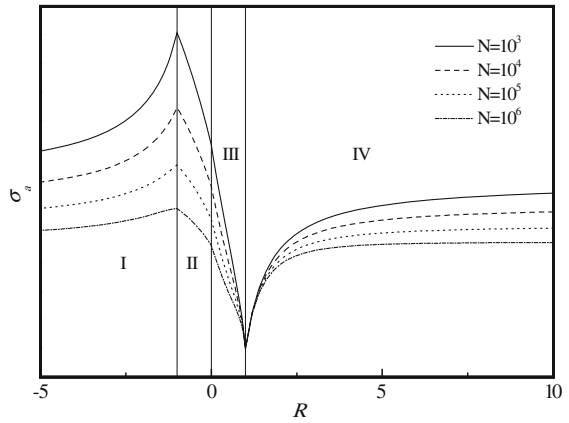

Fig. 4.22 Representation of constant life diagram on R–σ_a plane

rational explanation for the selection of these two stress parameters. Any other combination of σ_a–σ_m–R can just as well be used for the derivation of a constant life diagram. A plot of stress amplitude against stress ratio for different numbers of loading cycles is presented in Fig. 4.21.

The surface of Fig. 4.21 represents the fatigue failure locus of the examined material. Any loading combination above the surface causes failure. A projection of this surface on the R–σ_a plane can be considered as a constant life diagram, see Fig. 4.22.

In Fig. 4.22, the x-axis represents the R-ratio and ranges from $-\infty$ to $+\infty$ without any singularity. The y-axis represents the stress amplitude and has positive values. S–N curves for any stress ratio, R, are represented by vertical lines emanating from the corresponding value of R on the x-axis. This diagram can be divided into four distinct domains, each corresponding to different loading conditions: Domain I for compression-tension (C-T) loading under $-\infty \leq R \leq -1$, Domain II for tension-compression (T-C) loading under $-1 \leq R \leq 0$, Domain III

corresponding to T-T loading under $0 \leq R \leq 1$ and Domain IV for C-C loading under $1 \leq R \leq +\infty$.

The material's behavior in each of these domains can be described by simple phenomenological non-linear fitting equations and the model parameters can be estimated by using appropriate boundary conditions for each domain of the diagram and known values of σ_a, σ_m and R, as described in the following:

Domains *I and IV:* $-\infty \leq R \leq -1$ and $1 \leq R \leq +\infty$:

$$\sigma_a = (1-R)\left(\frac{A_{I,\text{or}\,IV}}{R} + \frac{B_{I,\text{or}\,IV}}{R^2}\right) \tag{4.25}$$

where A_I, B_I, A_{IV} and B_{IV} are model parameters that can be easily determined by fitting Eq. 4.26 to the available experimental data.

The process is based on the selection of the appropriate boundary conditions for each domain of the CLD. For Domains I and IV, described by Eq. 4.25, the boundary conditions are the following:

$$\begin{aligned} &\text{for } R=-1,\ \sigma_a = \sigma_a^{R=-1},\ \text{and } \sigma_m = 0, \\ &\text{for } R=\pm\infty,\ \sigma_a = \sigma_a^{R=\pm\infty},\ \text{and} \\ &\text{for } R=1,\ \sigma_a = 0,\ \text{and } \sigma_m = UCS \end{aligned} \tag{4.26}$$

where stress parameter superscripts denote the corresponding stress ratio, e.g. $\sigma_\alpha^{R=-1}$ is the stress amplitude for $R=-1$.

By applying these three boundary conditions, Eq. 4.25 becomes:

$$\begin{aligned} &\text{for } R=-1 \ \rightarrow\ \sigma_a^{R=-1} = 2(-A_I + B_I)\,,\ \text{or} \\ &\text{for } R=1 \ \rightarrow\ UCS = 2(A_{IV} + B_{IV})\,,\ \text{or} \\ &\text{for } R=\pm\infty \ \rightarrow\ \sigma_a^{R=\pm\infty} = \lim_{R\rightarrow\pm\infty}(1-R)\left(\frac{A_{I,\text{or}\,IV}}{R} + \frac{B_{I,\text{or}\,IV}}{R^2}\right) = -A_{I,\text{or}\,IV} \end{aligned} \tag{4.27}$$

and the four fitting parameters A_I, B_I, A_{IV} and B_{IV} can be defined as:

$$\begin{aligned} A_{I,\text{or}\,IV} &= -\sigma_a^{R=\pm\infty} \\ B_I &= \frac{\sigma_a^{R=-1}}{2} - \sigma_a^{R=\pm\infty} \\ B_{IV} &= \frac{UCS}{2} + \sigma_a^{R=\pm\infty} \end{aligned} \tag{4.28}$$

When the S–N curve under $R=10$ is available instead of that under $R=\pm\infty$, the boundary conditions should be adjusted accordingly.

Domains II and III: $-1 \leq R \leq 0$ and $0 \leq R \leq 1$:

$$\sigma_a = \frac{1-R}{A_{II,\text{or}III}R^n + B_{II,\text{or}III}} \tag{4.29}$$

The fitting of Eq. 4.29 on the constant amplitude fatigue data of several different material systems [39] proved that parameter n can be considered equal to 1 for Domain II and equal to 3 for Domain III. The boundary conditions are the following:

$$\begin{aligned} &\text{for } R = 1,\ \sigma_a = 0 \text{ and } \sigma_m = UTS \\ &\text{for } R = -1,\ \sigma_a = \sigma_a^{R=-1} \text{ and } \sigma_m = 0 \end{aligned} \tag{4.30}$$

if only the S–N curves under $R = -1$ and $R = 1$ are used. Implementing the above-mentioned boundary conditions results in:

$$\begin{aligned} A_{II,\text{or } III} &= \frac{1}{UTS} - \frac{1}{\sigma_a^{R=-1}} \\ B_{II,\text{or } III} &= \frac{1}{UTS} + \frac{1}{\sigma_a^{R=-1}} \end{aligned} \tag{4.31}$$

However, if the S–N curve under $R = 0$ is considered as well, the boundary conditions Eq. 4.31 are supplemented by:

$$\sigma_a = \sigma_a^{R=0},\ \text{for } R = 0 \tag{4.32}$$

By applying the boundary conditions for Domains II and III in Eq. 4.29, parameters A_{II}, B_{II}, A_{III} and B_{III} acquire the following values:

$$\begin{aligned} A_{II} &= \frac{1}{\sigma_a^{R=0}} - \frac{2}{\sigma_a^{R=-1}} \\ A_{III} &= \frac{2}{UTS} - \frac{1}{\sigma_a^{R=0}} \\ B_{II,\text{or } III} &= \frac{1}{\sigma_a^{R=0}} \end{aligned} \tag{4.33}$$

Similarly to Domains I and IV, when the S–N curve under $R = 0.1$ is available instead of that under $R = 0$, the boundary conditions are modified accordingly. More S–N curves may be used to improve the accuracy of the model. However, as shown in the next paragraphs, the use of only two or three S–N curves, under $R = -1$, $R = \pm\infty$ (alternatively $R = 10$), and $R = 0$ (alternatively $R = 0.1$) suffices to produce an accurate model.

The PNL constant life diagram for the on-axis specimens on the $(\sigma_m$–$\sigma_a)$-plane is presented in Fig. 4.23. The S–N curves derived under $R = 10$, -1 and 0.1 have been used for the calibration of the model.

4.3.2 Evaluation of the CLD Models

The performance of the examined constant life diagrams has been evaluated on three different material systems. In addition to the material examined in this book

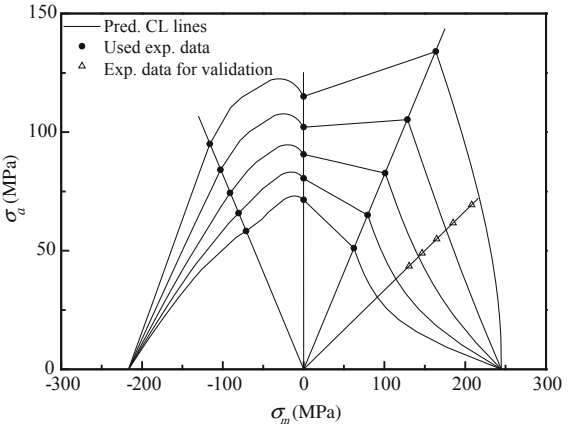

Fig. 4.23 PNL CLD for on-axis specimens, $N = 10^3$–10^7

(see Chap. 2), two more material databases were used in order to support the analysis and assist the derivation of more reliable conclusions. All examined materials are fiberglass-polyester and fiberglass-epoxy laminates, which are typical materials used in the wind turbine rotor blade construction industry.

The following criteria were considered to evaluate the applicability of the examined CLD models and assess their influence on the fatigue life prediction of the examined composite materials:

Accuracy of predictions: quantified by the accuracy of predicting new S–N curves.
Need for experimental data: quantified by the number of S–N curves required to apply each CLD model.
Difficulty of application: qualitative criterion.
Implemented assumptions: qualitative criterion.

For the application of the linear model, the $R = -1$ curve was used. For the construction of the Kawai CFL, the $R = -1$ curve (the closest to the critical one, since the S–N curves corresponding to the critical R-ratios (ca. -0.9 for the on-axis specimens and ca. -0.8 for the specimens cut at 45° off-axis) are not available) together with the static strengths were employed. In addition, the $R = -0.5$ curve was used for the modeling of material #3, since for this case the critical R-ratio was -0.63. For the application of the remaining models – piecewise linear, Harris and Boerstra—three to five S–N curves, under $R = 0.1$, $R = -1$, $R = 10$ and additionally $R = 0.5$ and $R = 2$ (for material #3) along with the static strengths were used to describe all the regions of the CLD. Kassapoglou's model was applied only for the database of material #3, since it was the only one for which a statistically significant population of static strength data was available. Power curve fitting was performed on all available experimental fatigue data to determine the S−N curves. These curves were used in all formulations in order to have the same basis for the comparisons.

Material #1 GFRP multidirectional specimens cut on-axis and at 45° off-axis from a laminate with the stacking sequence $[0/(\pm 45)_2/0]_T$ (from Chap. 2).

Specimens cut on-axis and at 45° from the multidirectional laminate from Chap. 2 were considered as the first example for the comparison of the CLD formulations. The selected test set consisted of 56 (for the on-axis) and 57 (for the off-axis) valid fatigue data points, distributed in four S–N curves per case (at ratios $R = 0.5, 0.1, -1$ and 10). This is a typical dataset containing experimental fatigue data for the initial steps of design processes. Details concerning the specified material, preparation and testing procedures can be found in Chap. 2 of this volume. The UTS and UCS for this material were experimentally determined by axial tests as being 244.84 MPa and 216.68 MPa for the on-axis and 139.12 MPa and 106.40 MPa for the 45° off-axis specimens.

Three of the four existing S–N curves and the static strength values were used as the input data. The S–N curve at $R = -1$ was used for the construction of the linear CLD and the Kawai CFL. For the model proposed by Boerstra, this is not necessary, as it can be applied even for sparse fatigue data in the $(\sigma_a–\sigma_m–N)$-space. However, the CLD based on the fitted S–N curves was also plotted. Pre-processing of the fatigue data revealed that Eq. 4.14 is more appropriate for determination of parameter f, as prescribed by the Harris model. Equations (4.12) and (4.13) were used for the u and v parameters. The resulting CLD based on the estimation of all parameters using Eqs. 4.11–4.13 was also derived for the comparisons.

Different CLDs based on the various approaches are presented in Figs. 4.16, 4.17, 4.18, 4.19, 4.20 and 4.23 for the on-axis specimens, and Fig. 4.24 for the 45° off-axis specimens. Based on the results, Linear and Kawai CLDs are inaccurate for the examined material, while the predictions of the piecewise linear and Boerstra diagrams at the stress ratio $R = 0.5$ seem the most accurate.

It should be mentioned that the S–N curve used as the critical one is different from that recommended by Kawai's model and this may be the reason for the inaccurate results. As shown in Fig. 4.24c, the influence of parameter f on the shape of the predicted CLD based on Harris's model is very important. Insufficient modeling of its relationship to fatigue life can introduce significant errors. However, use of both fitting equations, Eqs. 4.11–4.13 or Eq. 4.14, introduced errors, especially in the vicinity of the low-cycle fatigue region. The application of Boerstra's model based on the experimental results instead of the fitted S–N curves led to a less conservative CLD for the examined material. The accuracy is not significantly affected by this selection however.

Material #2 Multidirectional glass-polyester laminate with a stacking sequence that can be encoded as $[(\pm 45)_8/0_7]_S$, [46].

The second material used for the comparisons was a multidirectional glass-polyester laminate consisting of 50% per weight unidirectional and 50% per weight ±45 plies. The material data were initially produced for the FACT database and were subsequently included in the Optidat database [46]. A total of 101 valid fatigue data points were found for the predetermined material tested under

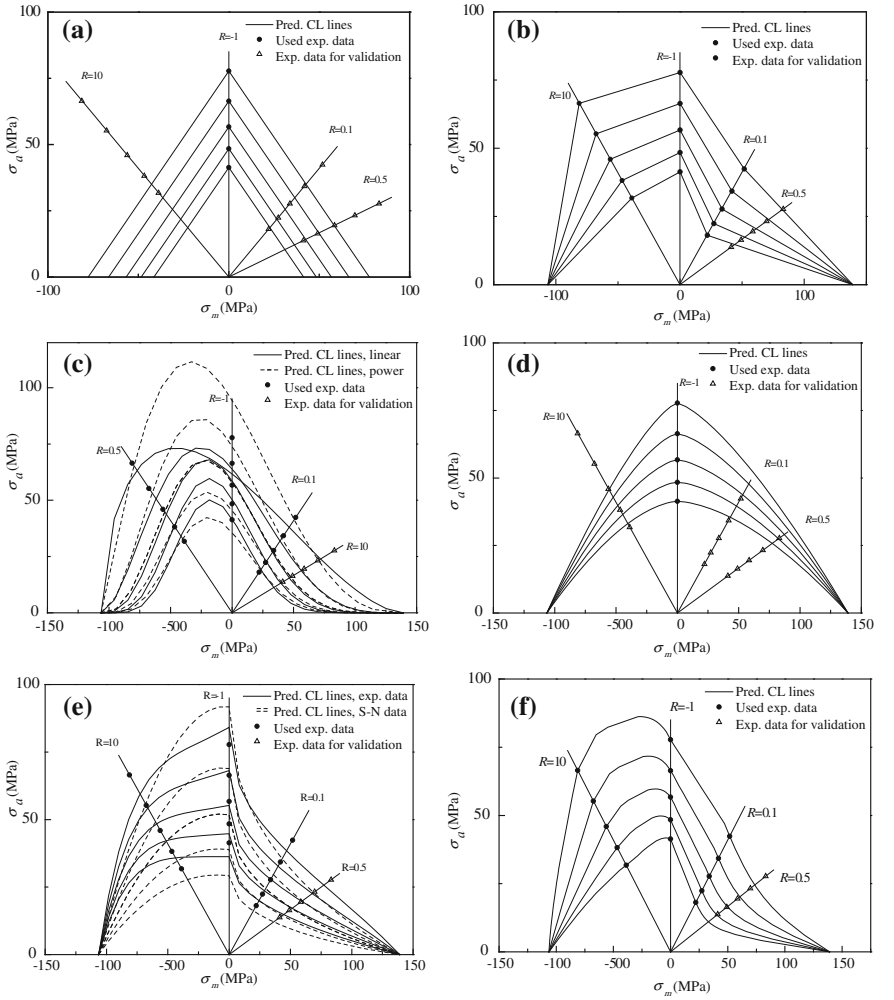

Fig. 4.24 Constant life diagrams for $N = 10^3$–10^7, material #1 (linear-a, piecewise linear-b, Harris-c, Kawai-d, Boerstra-e, piecewise non-linear-f)

five different constant amplitude conditions: $R = 0.1, -0.4, -1, 10, -2$ and used for comparisons. In this dataset, the maximum stress level ranged between 65 and 325 MPa and measured lifetime was between 48 for low-cycle fatigue, and 60.3 million cycles for longer lifetimes. A UTS of 370 MPa and UCS of 286 MPa were reported.

Three of the five existing S–N curves, those under $R = 10, -1$ and 0.1, plus the static strengths were used as input data. The remaining two S–N curves (under $R = -0.4$ and -2) were used to evaluate the modeling accuracy of the proposed methods. As for material #1, the $R = -1$ S–N curve was used for the construction

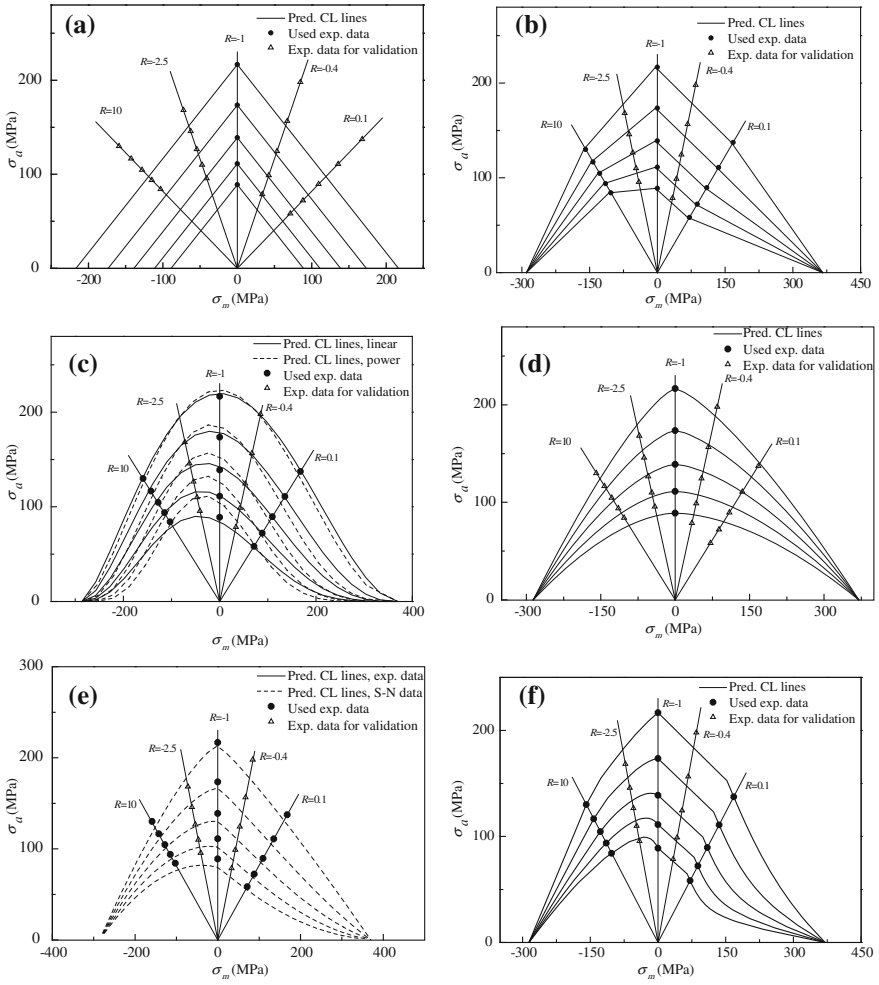

Fig. 4.25 Constant life diagrams for $N = 10^3$–10^7, material #2 (linear-a, piecewise linear-b, Harris-c, Kawai-d, Boerstra-e, piecewise non-linear-f)

of the linear and Kawai models, since it is the closest one to the critical stress ratio (−0.77). Based on the preprocessing of the experimental data, all model parameters for Harris were considered as linear functions of the log(N) and estimated by means of Eqs. 4.11–4.13.

Constant life diagrams according to the described models are presented in Fig. 4.25. All derived CLDs, except that prescribed by the linear model, are accurate for the prediction of the S–N curve at $R = -0.4$ and $R = -2.5$. As can be seen in Fig. 4.25e, the use of experimental data or fitted S–N data does not significantly affect the predictions based on Boerstra's model. The difference is even less when longer lifetime is evaluated.

Material #3 GFRP multidirectional laminate with a stacking sequence of $[90/0/\pm 45/0]_S$, [47].

The third example is based on experimental fatigue data retrieved from the DOE/MSU database, which has the code name DD16. The material was a multidirectional laminate consisting of eight layers, six of the stitched unidirectional material D155 and two of the stitched, ±45, DB120. CoRezyn 63–AX–051 polyester was used as the matrix material. The material was tested under 12 *R*-ratios for a comprehensive representation of a constant life diagram. Reading counterclockwise on the constant life diagram, the following *R*-ratios can be identified: 0.9, 0.8, 0.7, 0.5, 0.1, −0.5, −1, −2, 10, 2, 1.43 and 1.1.

Here, for comparison of the constant life formulations, experimental data collected under seven *R*-ratios (0.8, 0.5, 0.1, −0.5, −1, −2 and 10) were selected. In total, 360 valid constant amplitude fatigue data points were retrieved. The absolute maximum stress level during testing was between 85 and 500 MPa and the corresponding recorded cycles up to failure ranged from 37 cycles in the low-cycle fatigue region to 30.4 million in the high-cycle fatigue region. The UTS for this material was determined as 632 MPa, while the UCS was 402 MPa. More information about this material system and the testing conditions along with more data for further analyses can be found in [47].

Five of the seven existing S–N curves plus the static strengths were used as input data for all the CLDs, except for the linear and Kawai models which require only one S–N curve. The remaining two were used to evaluate the modeling accuracy of the proposed methods.

For material DD16, the strength ratio according to Kawai is −0.63. Therefore, the S–N curve at $R = -0.5$ was also used for the derivation of the CFL based on Kawai's instructions. Preprocessing of the experimental data showed that the behavior of parameter *f* in Harris's model can be better fitted by the power law given by Eq. 4.14. Equations 4.12 and 4.13 were used for the other two model parameters. However, application of the model based on the linear fitting of all three parameters was also performed. Power S−N curves were used for the implementation of all models, but again, Boerstra's CLD was constructed using the untreated experimental data as well.

Constant life diagrams according to the described models are presented in Fig. 4.26. The linear diagram is accurate only for the prediction of the curve at the stress ratio, $R = -0.5$ ($R^2 = 0.93$), but failed to accurately predict the curve at $R = 0.8$. The predictions of the piecewise linear diagram were better in both cases. The influence of the selection of the power or linear fitting for estimation of the parameter *f* in Harris's model is significant, as shown in Fig. 4.26c. The bad fitting quality of Eq. 4.11 for the derivation of the relationship between parameter *f* and number of loading cycles results in the inaccurate CLD presented in Fig. 4.26c. On the other hand, use of the S–N curve at $R = -0.5$, as being closest to the S–N curve determined as critical by Kawai, seems to improve the modeling accuracy, although not in a consistent manner. Furthermore, the application of Boerstra's model based on fitted S–N data significantly improved accuracy, especially for the

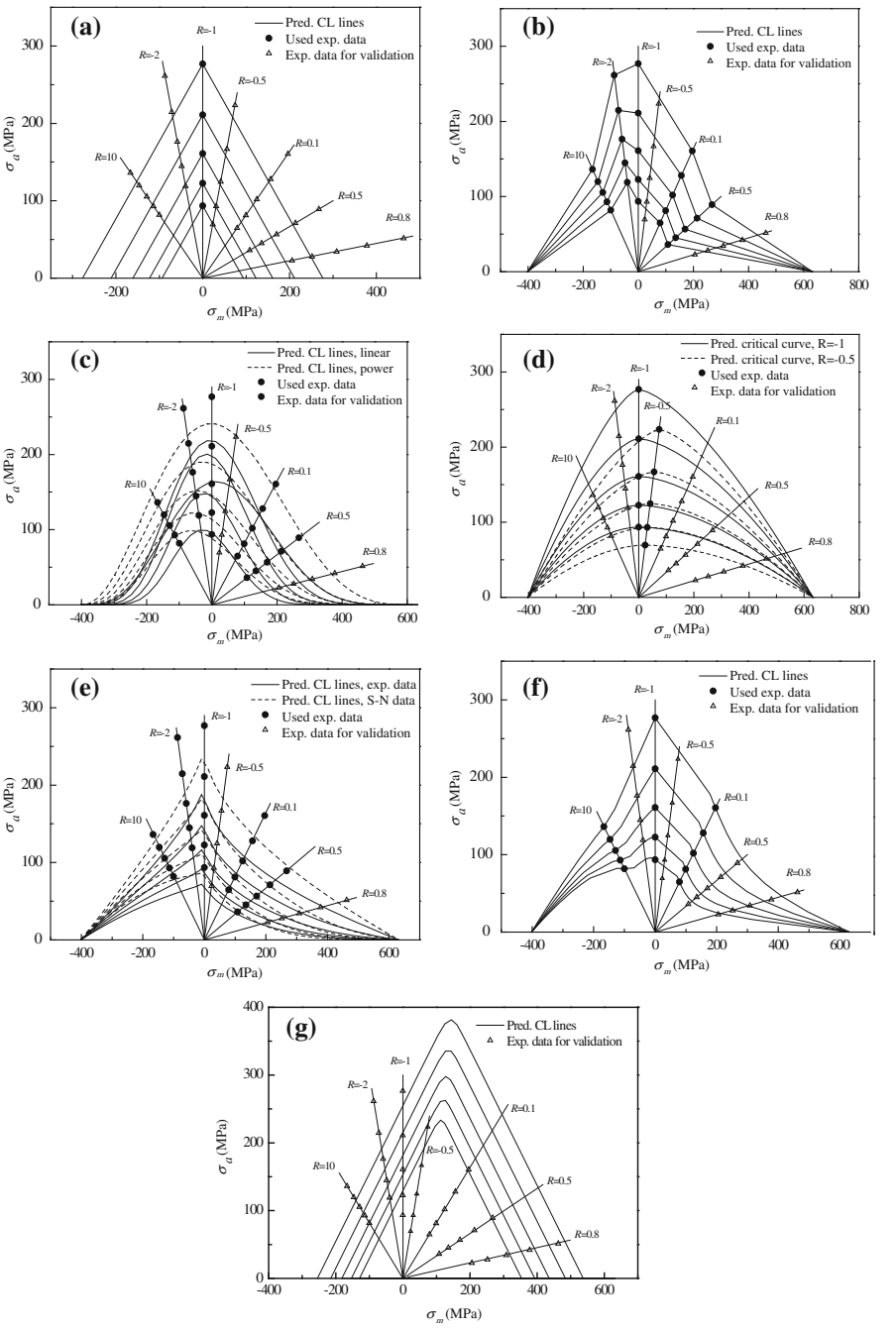

Fig. 4.26 Constant life diagrams for $N = 10^3$–10^7, material #3 (linear-a, piecewise linear-b, Harris-c, Kawai-d, Boerstra-e, piecewise non-linear-f, Kassapoglou-g)

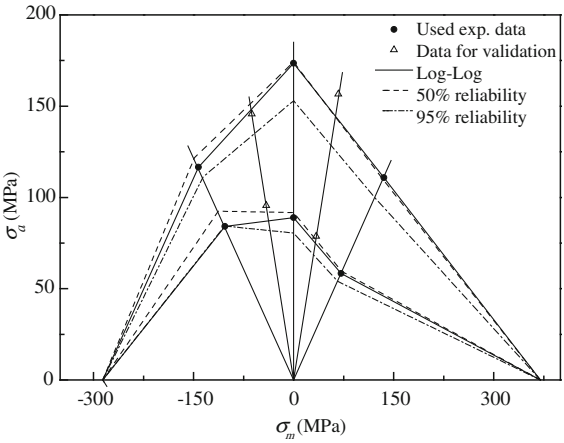

Fig. 4.27 Comparison of CLDs based on different S–N formulations and different reliability levels, material #2

S–N curve at $R = -0.5$. The model proposed by Kassapoglou produced very poor results.

All comparisons were based on the assumption that a power law-based equation, corresponding to a 50% reliability level, is appropriate for the accurate modeling of the constant amplitude fatigue data. However, any other S–N formulation, e.g., a mathematical expression that provides statistically based S–N curves [48] or even S–N curves estimated by using computational tools such as genetic programming [8] or neural networks [19], can be employed for the interpretation of the fatigue data. The piecewise linear CLD for material #2 would look like that shown in Fig. 4.27, if S–N curves for 50% and 95% reliability levels derived based on the method described in [48] and not based on the standard power low equation are used for interpretation of the fatigue data.

As can be seen, use of a different S–N formulation has a limited effect on the CLD shape, especially for numbers of cycles between 10^3 and 10^7. As was shown in [8], in this region most S–N formulations provide similar fatigue models, although a higher reliability level results in more conservative diagrams however.

4.3.2.1 Evaluation of CLD Performance

Comparison of the results shows that the piecewise linear, piecewise non-linear, Harris, Kawai and Boerstra CLD models can be sufficiently accurate under specific conditions. The linear model and the one proposed by Kassapoglou were proved to be inaccurate for the examined material's fatigue data. Comparison of the CLDs from the four eligible models reveals that piecewise linear is more consistent than the others since it is not based on any assumption. It is constructed by linear interpolation over the available fatigue data and therefore accurately depicts their behavior. The other three diagrams are very sensitive to the selection of the input data, especially Kawai, and estimation of the model parameters, e.g., Harris.

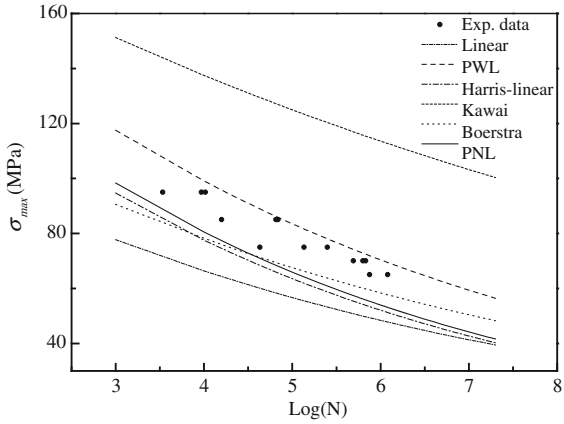

Fig. 4.28 Predicted S–N curves for $R = 0.5$, material #1

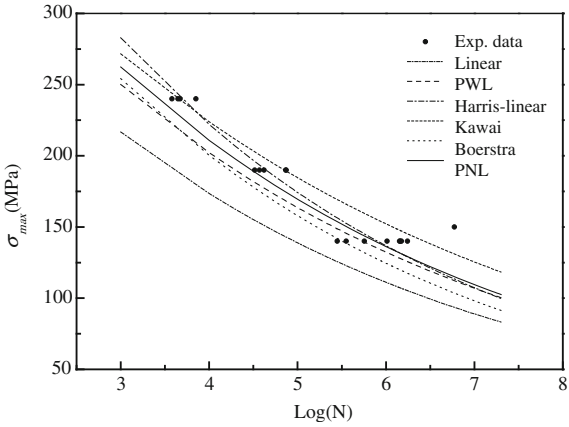

Fig. 4.29 Predicted S–N curves for $R = -0.4$, material #2

A graphical comparison of the predicting ability of the different CLD modeling methods is attempted in Figs. 4.28, 4.29, 4.30 and compared to the available experimental data for arbitrarily selected cases. The linear model underestimates the fatigue strength of the examined material in all the examined cases, leading to conservative fatigue life predictions. On the other hand, Kawai's model generally overestimates the behavior, implying an optimistic assessment of fatigue life and thus a non-conservative fatigue design. Although still not accurate, the predictions from the piecewise linear and the piecewise non-linear together with those derived by the Boerstra model seem to be the most representative of the fatigue behavior of the material under the specific loading pattern.

A quantification of the predicting ability of each of the applied models was performed. Table 4.2 shows the R^2 values between the predicted curves and the experimental data for validation.

Generally, higher values were exhibited by the piecewise non-linear followed by the piecewise linear formulation. These models seem to be the most reliable for

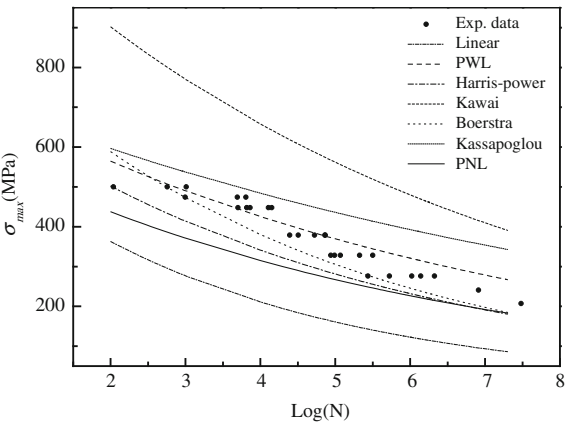

Fig. 4.30 Predicted S–N curves for $R = 0.8$, material #3

Table 4.2 Comparison of predicting ability of the applied models in terms of coefficient of multiple determination (R^2)

	Material #1	Material #2		Material #3		
	$R = 0.5$	$R = -0.4$	$R = -2.5$	$R = -1$	$R = -0.5$	$R = 0.8$
Linear	0.37	0.72	0.61	–	0.93	0.35
Piecewise linear	0.89	0.91	0.84	–	0.88	0.93
Harris−f: Linear	0.63	0.95	0.71	–	0.77	0.51
Harris−f: power law	0.64	0.94	0.64	–	0.94	0.80
Kawai ($R = -1$)	0.15	0.94	0.83	–	0.87	0.31
Kawai ($R = -0.5$)	–	–	–	0.76	–	0.43
Boerstra-Exp Data	0.65	0.86	0.83	–	0.60	0.85
Boerstra-SN Data	0.69	0.89	0.84	–	0.84	0.91
Kassapoglou	–	–	–	0.93	0.41	0.48
PNL	0.88	0.95	0.96		0.92	0.78

the entire set of data examined in the present chapter. Other CLD formulations can also be accurate, however, although not consistently so. Their accuracy depends on the quality of the examined fatigue data, the selected input data (e.g., linear, Kawai) and the quality of the fitting and/or optimization for estimation of the parameters (Harris and Boerstra).

In terms of need for experimental data, it is obvious that the model proposed by Kassapoglou is the least demanding, followed by the linear and Kawai models. However, as already discussed, this compromise reduces the accuracy of the predictions. The piecewise linear can also be implemented by using a single S–N curve, thus becoming equivalent to a shifted Goodman diagram, but, as mentioned above, in this case its predictive ability is also reduced.

As far as ease of application is concerned, the only difficulty occurs in the Harris and Boerstra models. According to the former, a non-linear regression should be performed for the derivation of the three-model parameters, while for

the latter, a five-parameter optimization problem must be solved to estimate desired constant lifelines.

Apart from the piecewise linear, all other models depend on a number of assumptions. These assumptions originate either from experience and experimental evidence, e.g., in the linear, Harris, Kawai and Boerstra models, or are clearly theoretical assumptions like the one introduced by Kassapoglou. As previously shown, the adoption of any assumption can simplify the models, which, under certain conditions, can produce quite accurate results.

However, there is no guarantee that these models can be used for different materials or even different loading patterns.

4.3.3 Concluding Remarks Regarding the CLD Performance

A comparison of the commonly used and recently developed models for the derivation of constant life diagrams for composite materials was carried out in this section. Seven methods were described, and their prediction accuracy was evaluated over a wide range of constant amplitude fatigue data obtained from GFRP materials. The influence of the selection of the CLD method on the fatigue life prediction of composite materials was quantified. The following conclusions were drawn:

- The selection of an accurate CLD formulation is essential for the overall accuracy of a fatigue life prediction methodology. As shown, the "wrong" choice can produce very conservative or very optimistic S–N curves, which is directly reflected in the corresponding life assessment.
- All methods involve the problem of mixing static and fatigue data. Their accuracy is reduced when curves close to $R = 1$ (in tension or compression) have to be predicted. Moreover, the same applies for the derivation of accurate S–N curves to describe the very low-cycle fatigue regime, i.e., $N < 100$. The unified equation used in Harris's model to describe fatigue behavior for both tension and compression loading also includes the influence of the damage mechanisms that developed under different loading patterns. All other models work separately for tension and compression loading; they are based on different equations for the description of different parts of the constant life diagram.
- The simplicity offered by some of the models, e.g., linear, Kassapoglou, Kawai, in most cases compromises accuracy. In addition, although these models were developed with the aim of minimizing the amount of experimental data required, they do not offer the possibility of using more data when an extensive database is available, e.g., linear and Kawai are based on the critical S–N curve and cannot accommodate any other S–N curves in order to improve the accuracy of the predictions. Another deficiency of models like these two is that they cannot be used to analyze random variable amplitude fatigue loading with continuously changing mean and amplitude, since they are accurate only

for S–N curves close to the critical one (for the linear) and only if the critical one (according to the material) can be experimentally derived (Kawai). It should be mentioned however, that Kawai introduced his model for the description of CFRP material behavior different from that of the GFRP materials examined in this study.

- The accuracy of Harris's model is acceptable only when the behavior of the model parameters can be effectively fitted versus the fatigue life. However, the fitting methods proposed by Harris do not always lead to accurate results.
- Boerstra's model can be used without the need to fit the available experimental data with an S–N curve. This is an asset since it can therefore be used to model variable amplitude data with continuously varying mean and amplitude values. However, it was proved that use of the fitted S–N data instead improves the modeling accuracy of the Boerstra model.
- The relatively simple piecewise linear and its non-linear counterpart, the PNL, were proved the most accurate of the compared formulations when a reasonable number of S–N curves ($\geq$2–3) is available. A more sophisticated, non-linear interpolation between the known S–N values and a more realistic description of the behavior close to $R = 1$ would improve the results of these models.

4.4 Stiffness Degradation

The stiffness/strength-based models were mostly established as phenomenological models since they propose an evolutionary law to describe the gradual degradation of the specimen's stiffness or strength in terms of macroscopically measurable properties [49]. The modeling of the varying damage metric reflects the damage accumulation in specimens during fatigue. The damage metric depends on many factors, including applied cyclic stress, number of fatigue cycles, loading frequency and environmental conditions.

The stiffness-based model is derived from the change in stiffness of a material or a structural component undergoing fatigue. The residual stiffness is expressed as a function of initial stiffness and number of cycles. The relationship between these three parameters can be of any mathematical form, e.g., linear, power, sigmoid, depending on the experimental data. Similar models were developed using residual strength as the damage metric. However, stiffness offers certain advantages compared to strength: it can be measured using non-destructive methods and presents less scatter on the measured results than strength data. Furthermore, residual strength exhibits only minimal decreases with the number of cycles until it begins to change rapidly close to the end of lifetime, while stiffness exhibits greater changes during fatigue life [50–53] and thus a higher sensitivity to damage progression.

A wide variety of composite materials exhibit a stiffness degradation trend that can be simulated by a curve like the one schematically shown in Fig. 4.31.

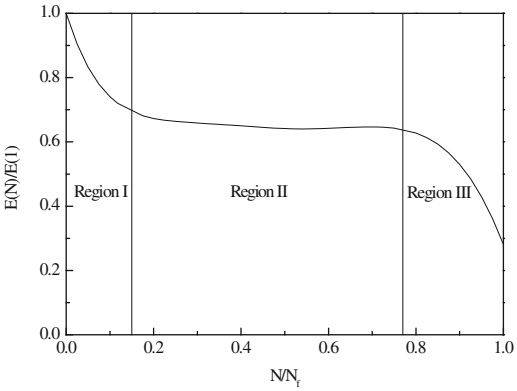

Fig. 4.31 Schematic representation of a typical stiffness degradation curve for composite materials

The three regions designated in this figure were firstly distinguished by Schulte for the tension-tension fatigue of cross-ply carbon/epoxy laminates [54].

In the initial region, and up to around 10% of fatigue life, the material exhibits a sudden stiffness reduction (compared to region II). In the intermediate region, the material's stiffness degrades at a constant and moderate rate. Finally, significant deterioration of the material can be observed close to the end of the fatigue life. A third region with a steeply descending slope simulates this phenomenon.

The main objective of the research community is to model this behavior for any selected composite material for different structural applications. To this end, a power law relationship was used in [55, 56] to describe the stiffness degradation of a glass-fiber cloth composite laminate and the concept of fatigue modulus was introduced. It was defined as the ratio of maximum stress over maximum strain at a specific cycle. The fatigue modulus measured during the first loading cycle was assumed to be the same as the elastic modulus. The fatigue modulus at failure was dependent on the applied cyclic stress level.

A modified exponential model was introduced in [3] to describe the behavior of graphite/epoxy laminates. Stiffness at any loading cycle was expressed as a function of the initial stiffness, ultimate strength of the laminate, applied stress level and two constants that should be adjusted by fitting the model to the experimental data.

Although a number of studies have been presented on the modeling of the stiffness degradation of several materials, fewer have been presented on the investigation of the fatigue behavior of structural components such as structural joints, e.g., [57, 58].

The concept of the shear stiffness modulus was introduced in [57] for the study of the fatigue life of adhesive lap joints produced from bi-directional woven E-glass fibers and polypropylene matrix. The shear stiffness modulus was defined as the ratio between shear stress in the bond and axial strain. Experimental results showed that the joints exhibited little and almost linear stiffness degradation throughout most of their life, followed by a sudden decrease between $0.95 < N/N_f < 1$. A similar tendency was observed in [58] for double-lap

joints composed of GFRP pultruded laminates. Although GFRP laminates exhibited considerable stiffness degradation under low cyclic loads, the joint specimens showed degradation of less than 5% failure. Two empirical models, a linear and a non-linear, were introduced in [59] for the modeling of the stiffness degradation of two types of joints commonly used in civil engineering applications, and the derivation of design allowables for the examined structural joints based on stiffness degradation measurements.

The above-mentioned studies proved that residual stiffness could be an efficient damage metric for the description of the fatigue behavior of composite materials and structures. Based on this metric, fatigue design curves can be derived that do not correspond to failure but to a certain percentage of specimen stiffness reduction. This concept was initially introduced in [60] where the author proposed the derivation of S–N curves corresponding to specific stiffness degradation. In this case, data points in the S–N plane denote that under cyclic stress a predetermined stiffness reduction is reached after N cycles. Such stiffness-controlled fatigue design curves, henceforth denoted by Sc-N, can be derived in a straightforward manner using empirical stiffness degradation models, like the simple one previously introduced in [61]. The accuracy of this theoretical approach has been validated independently using experimental data from different material systems [62].

Especially for the design of structures containing rotating parts, like wind turbine or helicopter rotor blades, Sc-N curves can better serve the requirements of proposed full-scale testing procedures [63], where blade functional failure is said to correspond to irreversible stiffness reduction of up to 10%. Therefore, to conform to this kind of testing procedure for example, fatigue design allowables in the form of Sc-N curves must be established, and to that end systematic stiffness reduction data monitoring and statistical analysis must be performed beforehand.

In the following, the experimental data presented in Chap. 2 will be used for the demonstration of a method for the derivation of Sc-N curves, and the modeling of the fatigue life of the examined material. Sc-N curves determined for each R-value and off-axis direction will be compared to fatigue strength ones-N curves derived based on the statistical analysis of the fatigue strength data.

4.4.1 Fatigue Life Modeling Based on Stiffness Degradation

Although more complicated and therefore more accurate models for the modeling of stiffness variations during fatigue life exist [54], the simple empirical model for the description of stiffness changes and the derivation of stiffness-controlled design curves previously introduced in [61] and further validated for different material systems in [62] is used here for the demonstration of the technique. A brief outline of the model is given below.

The degree of damage in a polymer matrix composite coupon can be evaluated by measuring stiffness degradation, $E(N)/E(1)$, where $E(1)$ denotes the Young's

modulus of the material measured at the first cycle, different in general from the static value, E_{st}, and $E(N)$ is the Young's modulus measured at the N-th cycle. It is assumed that stiffness degradation can be expressed by [53]:

$$\frac{E(N)}{E(1)} = 1 - k_1 \left(\frac{\sigma_a}{E_{st}}\right)^{k_2} N \tag{4.34}$$

Material constants, k_1 and k_2, in Eq. 4.34 are determined by curve fitting of the respective experimental data for $E(N)/E(1)$, which depend on the number of stress cycles, N, and the level of applied cyclic stress amplitude, σ_a. Rearranging Eq. 4.34 in the following form:

$$\frac{1 - \frac{E(N)}{E(1)}}{N} = k_1 \left(\frac{\sigma_a}{E_{st}}\right)^{k_2} \tag{4.35}$$

allows the easy determination of model constants.

Equation (4.34) also establishes a stiffness-based design criterion since for a predetermined value of $E(N)/E(1)$, e.g., p, one can solve for σ_a to obtain an alternative form of design curve, Sc-N, corresponding not to material failure but to a specific stiffness degradation percentage $(1 - p)\%$.

Sc-N curves for any specific stiffness degradation level, $E(N)/E(1)$, can be easily calculated by means of the following equation:

$$\sigma_a = E_{st} \left(\frac{1 - \frac{E(N)}{E(1)}}{k_1 N}\right)^{\frac{1}{k_2}} \tag{4.36}$$

4.4.2 Stiffness-Based and Reliability S–N Curves

Based on stiffness degradation data (Chap. 2), stiffness-controlled Sc-N curves, corresponding to specific $E(N)/E(1)$ values, were calculated by means of Eq. 4.36. Fatigue strength curves were also defined at predetermined survival probability values using Eq. 4.4 and parameters of the statistical model shown in Table 4.1.

When comparing these two kinds of fatigue design curves it is concluded that there is a correlation between the probability level of the fatigue strength curves and the stiffness degradation level of the Sc-N curves. To any survival probability level, $P_S(N)$, there is a corresponding unique stiffness degradation value, $E(N)/E(1)$, which can be determined from the cumulative distribution function of the respective stiffness degradation data. It is this value of $E(N)/E(1)$ for which the cumulative distribution function, $F(E(N)/E(1))$, takes the value of $P_S(N)$. For example, $F(E(N)/E(1)) = 0.95$ for a residual stiffness of 0.96 for 15° off-axis specimens loaded under $R = 0.1$, as shown in Fig. 4.28, and therefore, the Sc-N curve for $E(N)/E(1) = 0.96$ is corroborated well by the fatigue strength curve

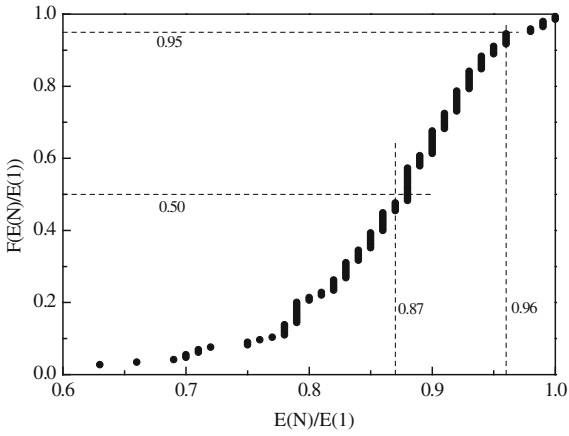

Fig. 4.32 Sampling distribution of stiffness degradation data, $R = 0.1$, 15° off-axis

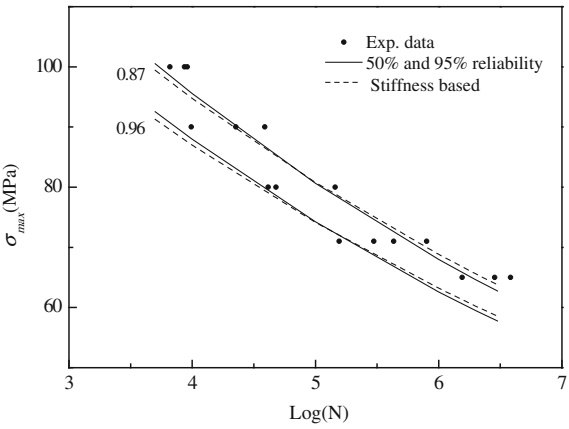

Fig. 4.33 Sc-N vs. S–N curves. $R = 0.1$, 45° off-axis

corresponding to a 95% reliability level as shown in Fig. 4.29. The same applies for the reliability level of 50%, a residual stiffness of 0.87 corresponds to this value of cumulative distribution function (see Fig. 4.32). It is indeed observed that Sc-N and S–N curves from each set lie very close to each other and that the former type of design curve is slightly more conservative. Using the Sc-N at $E(N)/E(1) = 0.96$ as derived from Fig. 4.32 as design allowable, a reliability level of at least 95% is guaranteed while stiffness reduction will be less than 5%. Similar comments are also valid for Figs. 4.33, 4.34 where corresponding curves are shown for specimens cut at different off-axis angles and tested under different R-ratios.

Observing the two different curves derived as stated in the above, it was concluded that they are similar for all cases considered in this work, with the Sc-N being slightly more conservative in general. Therefore, in design an Sc-N curve providing information on both survival probability and residual stiffness can be used.

It should be mentioned that this good correlation between stiffness-based and reliability S–N curves applies to all other types of specimens, tested under different

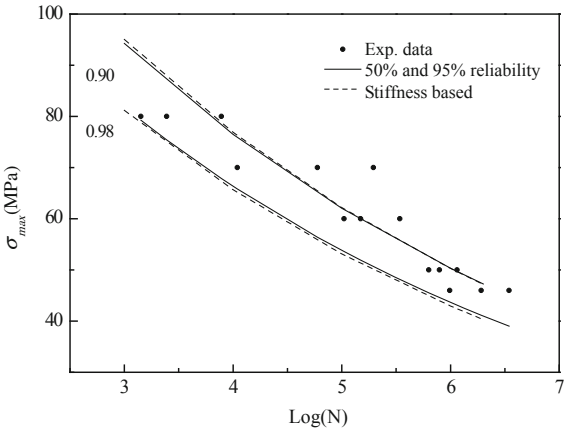

Fig. 4.34 Sc-N vs. S–N curves. $R = 10$, 90° off-axis

loading conditions. In Table 4.3, S–N curve equations are given for a 95% reliability level (according to Whitney's method, see Chap. 3) for all datasets used in this study and are compared to the corresponding stiffness-based Sc-N curve equations.

Despite the observed discrepancies, which are not significant in most cases, stiffness-based Sc-N curves can be used instead of reliability S–N curves in design. Curves of the former type provide information regarding two design parameters, reliability and stiffness degradation level. Thus, they can be used in design to fulfill the requirements of design codes and regulations. In addition, Sc-N curves can be determined much faster, as stiffness degradation trends are readily captured by testing only a small number of specimens.

To demonstrate this, the procedure for the determination of stiffness-based Sc-N curves was repeated by using only half of the specimens. Half of the specimens from each set was randomly selected and the calculations were repeated. The Sc-N curves determined in this way were then compared to the original ones. The probability cumulative distributions were almost identical in most of the cases studied, e.g., see Fig. 4.32. Thus, the Sc-N curves were similar to those determined by using the full dataset as shown for example in Fig. 4.35 for 30° off-axis coupons, tested under alternating stress, $R = -1$. (Figures 4.36, 4.37).

4.4.3 Concluding Remarks

During operational life, the stiffness of a structural element is reduced. The modeling of the fatigue life of specimens cut at several off-axis angles from a multidirectional laminate $[0/(\pm 45)_2/0]_T$ and subjected to uniaxial cyclic loading over a wide range of R-ratios was performed in this chapter based on stiffness degradation measurements.

A simple empirical model was used for the determination of design curves, which do not correspond to fatigue strength but to a predetermined value of

Table 4.3 Stiffness-controlled and S–N curves for 95% survival probability*

Direction	*R*-ratio							
	10		−1		0.1		0.5	
	Sc-N	S–N	Sc-N	S–N	Sc-N	S–N	Sc-N	S–N
0°	305.1 $N^{-0.0591}$ (0.97)	244.51 $N^{-0.0387}$	164.6 $N^{-0.0585}$ (0.98)	142.2 $N^{-0.0463}$	585.4 $N^{-0.1116}$ (0.85)	528.5 $N^{-0.1008}$	366.4 $N^{-0.0502}$ (0.95)	326.4 $N^{-0.0420}$
15°					168.2 $N^{-0.0733}$ (0.96)	164.9 $N^{-0.0694}$		
30°	327.7 $N^{-0.1139}$ (0.99)	321.9 $N^{-0.1115}$	113.2 $N^{-0.0807}$ (0.96)	113.8 $N^{-0.0788}$				
45°	216.9 $N^{-0.0758}$ (0.98)	238.8 $N^{-0.0843}$	133.4 $N^{-0.0850}$ (0.95)	112.9 $N^{-0.0721}$	161.6 $N^{-0.0950}$ (0.98)	153.4 $N^{-0.0921}$	166.9 $N^{-0.0719}$ (0.93)	156.96 $N^{-0.0671}$
60°	154.2 $N^{-0.0953}$ (0.98)	143.5 $N^{-0.0833}$	121.7 $N^{-0.0986}$ (0.89)	121.8 $N^{-0.0993}$				
75°					94.47 $N^{s0.0995}$ (0.83)	75.03 $N^{-0.0769}$		
90°	67.20 $N^{-0.0441}$ (0.99)	70.39 $N^{-0.0485}$		77.46 $N^{-0.0712}$	70.62 $N^{-0.0963}$ (0.84)	55.41 $N^{-0.0690}$		

* Numbers in parentheses indicate the respective $E(N)/E(1)$ values

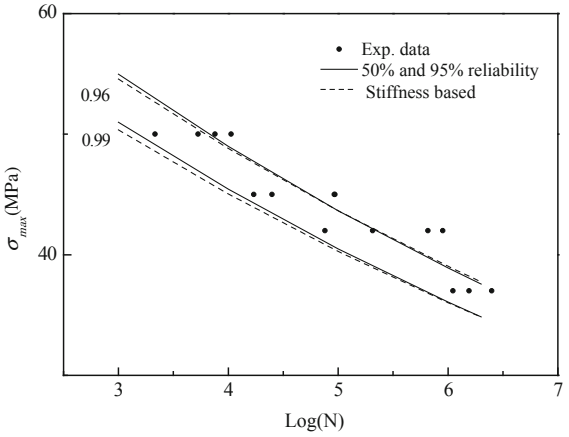

Fig. 4.35 Sc-N vs. S–N curves. $R = 0.1$, 15° off-axis

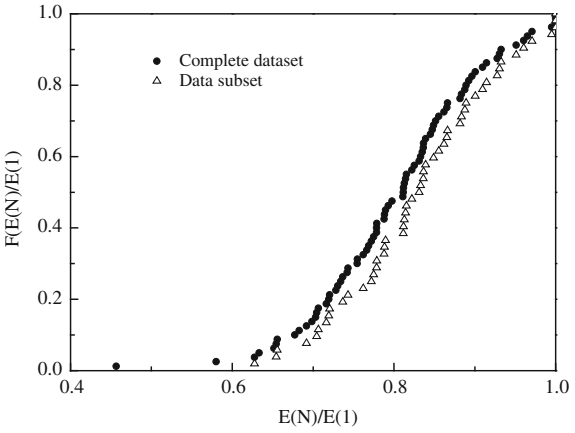

Fig. 4.36 Sampling distributions of complete and half of dataset. $R = -1$, 30° off-axis

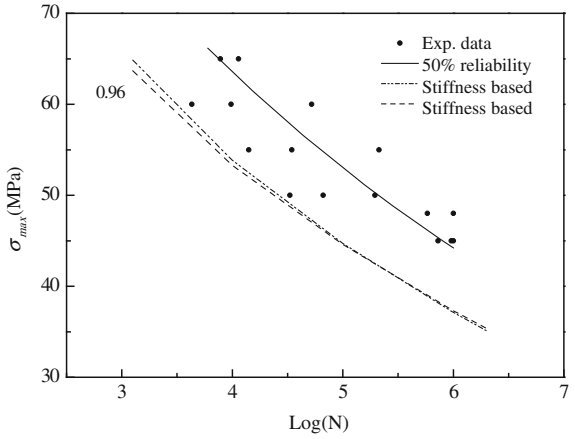

Fig. 4.37 Comparison of Sc-N curves determined using all and half of experimental stiffness degradation data

stiffness reduction by using only a portion of the fatigue data required for the determination of a reliable S–N curve. The established Sc-N curves provide information on the allowable stiffness degradation and also the probability of survival. It was shown that Sc-N curves are comparable to corresponding design allowables derived after statistical analysis of the fatigue strength data, although stiffness-controlled curves are, in most of the cases studied, slightly more conservative, especially for higher numbers of cycles.

4.5 Conclusions

Methods for the modeling of the constant amplitude fatigue life of composite materials and structures have been reviewed in this chapter. The traditional representation of the constant amplitude fatigue data on the S–N plane has been addressed in the first sections. Novel techniques that can be used for the derivation of more accurate S–N curve types were introduced and their modeling accuracy has been compared with that of conventional ways of representing fatigue data.

Constant life diagrams are commonly used for the prediction of "unseen" material data, under different loading conditions from those for which experimental constant amplitude fatigue data exist. The concept of the CLDs has been presented in this chapter and conclusions about their predicting ability have been drawn.

Modeling of the fatigue life of fiber-reinforced composite materials based on non-destructive measurements of the material stiffness and its fluctuations during fatigue life has long been a subject of investigation. A simple model has been employed in this chapter for the demonstration of a method that allows the derivation of stiffness-controlled S–N curves that represent the material's constant life fatigue behavior by accommodating both strength and stiffness information. The use of this method enables the testing time required to obtain fatigue design allowables, corresponding to a preset stiffness degradation and reliability level, to be reduced by at least 50%.

References

1. Z. Hashin, A. Rotem, A fatigue failure criterion for fiber–reinforced materials. J. Compos. Mater. **7**(4), 448–464 (1973)
2. H. El Kadi, F. Ellyin, Effect of stress ratio on the fatigue failure of fiberglass reinforced epoxy laminae. Composites **25**(10), 917–924 (1994)
3. H.A. Whitworth, A stiffness degradation model for composite laminates under fatigue loading. Compos. Struct. **40**(2), 95–101 (1997)
4. M. Kawai, S. Yajima, A. Hachinohe, Y. Takano, Off–axis fatigue behavior of unidirectional carbon fiber–reinforced composites at room and high temperatures. J. Compos. Mater. **35**(7), 545–576 (2001)
5. N.L. Post, Reliability based design methodology incorporating residual strength prediction of structural fiber reinforced polymer composites under stochastic variable amplitude fatigue

loading, PhD Thesis, Virginia Polytechnic Institute and State University, March 18, Blacksburg, Virginia (2008)
6. A.P. Vassilopoulos, R. Bedi, Adaptive neuro-fuzzy inference system in modeling fatigue life of multidirectional composite laminates. Comp. Mater. Sci. **43**(4), 1086–1093 (2008)
7. A.P. Vassilopoulos, E.F. Georgopoulos, T. Keller, Genetic programming in modeling of fatigue life of composite materials. in *13th International Conference on Experimental Mechanics-ICEM13: Experimental Analysis of Nano and Engineering Materials and Structures, Alexandroupolis*, Greece, July 1–6, 2007
8. A.P. Vassilopoulos, E.F. Georgopoulos, T. Keller, Comparison of genetic programming with conventional methods for fatigue life modeling of FRP composite materials. Int. J. Fatigue **30**(9), 1634–1645 (2008)
9. R.P.L. Nijssen, O Krause, T.P Philippidis, Benchmark of lifetime prediction methodologies, Optimat blades technical report, 2004, OB_TG1_R012 rev.001, http://www.wmc.eu/public_docs/10218_001.pdf
10. T. Adam, G. Fernando, R.F. Dickson, H. Reiter, B. Harris, Fatigue life prediction for hybrid composites. Fatigue **11**(4), 233–237 (1989)
11. J.A. Epaarachchi, P.D. Clausen, An empirical model for fatigue behavior prediction of glass fiber reinforced plastic composites for various stress ratios and test frequencies. Compos. Part A-Appl. Sci. **34**(4), 313–326 (2003)
12. J.M. Whitney Fatigue characterization of composite materials. in *Fatigue of Fibrous Composite Materials*, ASTM STP 723, American Society for Testing and Materials, 1981, 133–151
13. G.P. Sendeckyj, Fitting models to composite materials, in *Test methods and design allowables for fibrous composites, (ASTM STP 734*, ed. by C.C. Chamis (American Society for Testing and Materials, West Conshohocken, PA, 1981), pp. 245–260
14. J.A. Lee, D.P. Almond, B. Harris, The use of neural networks for the prediction of fatigue lives of composite materials. Compos. Part A-Appl. Sci. **30**(10), 1159–1169 (1999)
15. Y. Al-Assaf, H. El Kadi, Fatigue life prediction of unidirectional glass fiber/epoxy composite laminae using neural networks. Compos. Struct. **53**(1), 65–71 (2001)
16. J.A. Lee, D.P. Almond, A neural-network approach to fatigue-life prediction, in *Fatigue in composites*, ed. by B. Harris (Woodhead Publishing Ltd, Cambridge, UK, 2003), pp. 569–589
17. A.P. Vassilopoulos, E.F. Georgopoulos, V. Dionysopoulos, Modeling fatigue life of multidirectional GFRP laminates under constant amplitude loading with artificial neural networks. Adv. Compos. Lett. **15**(2), 43–51 (2006)
18. R.C.S.F. Junior, A.D.D. Neto, E.M.F. Aquino, Building of constant life diagrams of fatigue using artificial neural networks. Int. J. Fatigue **27**(7), 746–751 (2005)
19. A.P. Vassilopoulos, E.F. Georgopoulos, V. Dionysopoulos, Artificial neural networks in spectrum fatigue life prediction of composite materials. Int. J. Fatigue **29**(1), 20–29 (2007)
20. C.S. Lee, W. Hwang, H.C. Park, K.S. Han, Failure of carbon/epoxy composite tubes under combined axial and torsional loading 1. Experimental results and prediction of biaxial strength by the use of neural networks. Compos. Sci. Technol. **59**(12), 1779–1788 (1999)
21. J. Jia, J.G. Davalos, An artificial neural network for the fatigue study of bonded FRP-wood interfaces. Compos. Struct. **74**(1), 106–114 (2006)
22. M.A. Jarrah, Y. Al-Assaf, H. El Kadi, Neuro-Fuzzy modeling of fatigue life prediction of unidirectional glass fiber/epoxy composite laminates. J. Compos. Mater. **36**(6), 685–699 (2002)
23. AIM Learning Technology, http://www.aimlearning.com, last update 10.01.2007
24. J.R. Koza, *Genetic Programming on the Programming of Computers by Means of Natural Selection* (MIT Press, Cambridge, MA, 1992)
25. J.R. Koza, Genetic Programming, in *Encyclopaedia of Computer Science and Technology*, ed. by J.G. Williams, A. Kent (Marcel-Dekker, NY, 1998), pp. 29–43. 39. Supplement 24
26. V. Babovic, M. Keijzer, Genetic programming as a model induction engine. J. Hydroinform **2**(1), 35–60 (2000)
27. A.P. Vassilopoulos, B.D. Manshadi, T. Keller, Influence of the constant life diagram formulation on the fatigue life prediction of composite materials. Int. J. Fatigue **32**(4), 659–669 (2009)

28. N. Gathercole, H. Reiter, T. Adam, B. Harris, Life prediction for fatigue of T800/5245 carbon fiber composites: I. Constant amplitude loading. Int. J. Fatigue **16**(8), 523–532 (1994)
29. M.H. Beheshty, B. Harris, A constant life model of fatigue behavior for carbon fiber composites: the effect of impact damage. Compos. Sci. Technol. **58**(1), 9–18 (1998)
30. M. Kawai, M. Koizumi, Nonlinear constant fatigue life diagrams for carbon/epoxy laminates at room temperature. Compos.: Part A **38**(11), 2342–2353 (2007)
31. J.F. Mandell, D.D. Samborsky, L. Wang, N.K. Wahl, New fatigue data for wind turbine blade materials. J. Sol. Energy Eng. Trans. ASME **125**(4), 506–514 (2003)
32. H.J. Sutherland, J.F. Mandell, Optimized constant life diagram for the analysis of fiberglass composites used in wind turbine blades. J. Sol. Energy Eng. Trans. ASME **127**(4), 563–569 (2005)
33. T.P. Philippidis, A.P. Vassilopoulos, Complex stress state effect on fatigue life of GFRP laminates Part I, Experimental. Int. J. Fatigue **24**(8), 813–823 (2002)
34. B. Harris, A parametric constant-life model for prediction of the fatigue lives of fiber-reinforced plastics, in *Fatigue in Composites*, ed. by B. Harris (Woodhead Publishing Limited, Cambridge, UK, 2003), pp. 546–568
35. M. Kawai, A method for identifying asymmetric dissimilar constant fatigue life diagrams for CFRP laminates. Key. Eng. mater. **334–335**, 61–64 (2007)
36. G.K. Boerstra, The multislope model: a new description for the fatigue strength of glass reinforced plastic. Int. J. Fatigue **29**, 1571–1576 (2007)
37. C. Kassapoglou, Fatigue life prediction of composite structures under constant amplitude loading. J. Compos. Mater. **41**(22), 2737–2754 (2007)
38. C. Kassapoglou, Fatigue of composite materials under spectrum loading. Compos. Part A-Appl. Sci. **41**(5), 663–669 (2010)
39. A.P. Vassilopoulos, B.D. Manshadi, T. Keller, Piecewise non-linear constant life diagram formulation for FRP composite materials. Int. J. Fatigue **32**(10), 1731–1738 (2010)
40. W.Z. Gerber, Bestimmung der zulässigen spannungen in eisen-constructionen (Calculation of the allowable stresses in iron structures). Z Bayer Archit. Ing-Ver **6**(6), 101–110 (1874)
41. J. Goodman, *Mechanics Applied to Engineering* (Longman Green, Harlow, 1899)
42. V.A. Passipoularidis, T.P. Philippidis, A study of factors affecting life prediction of composites under spectrum loading. Int. J. Fatigue **31**, 408–417 (2009)
43. T.P. Philippidis, A.P. Vassilopoulos, Life prediction methodology for GFRP laminates under spectrum loading. Compos Part A–Appl S **35**(6), 657–666 (2004)
44. Awerbuch J, Hahn HT. Off-axis fatigue of graphite/epoxy composite. in *Fatigue of Fibrous Composite Materials. ASTM STP 723*, (American Society for Testing and Materials, 1981), pp. 243–273
45. M. Kawai, T. Murata, A three-segment anisomorphic constant life diagram for the fatigue of symmetric angle-ply carbon/epoxy laminates at room temperature. Compos Part A-Appl S **41**(10), 1498–1510 (2010)
46. Nijssen RPL. OptiDAT–fatigue of wind turbine materials database, 2006. <http://www.kc-wmc.nl/optimat_blades/index.htm>
47. Mandell JF, Samborsky DD. DOE/MSU Composite Material Fatigue Database. Sandia National Laboratories, SAND97-3002 (online via www.sandia.gov/wind, v. 18, 21st March 2008 Updated)
48. G.P. Sendeckyj. Fitting models to composite materials fatigue data. Test Methods and Design Allowables for Fibrous Composites. ASTM STP 734. C.C. CHAMIS, editor. American Society for Testing and Materials, 1981. p. 245–260
49. J. Degrieck, W.M. Paepegem, Fatigue damage modeling of fiber-reinforced composite materials: a review. Appl. Mech. Rev. **54**(4), 279–300 (2001)
50. G.P. Sendeckyj. Life prediction for resin-matrix composite materials. in *Fatigue of Composite Materials*, ed. by K.L. Reifsneider, Composite Materials Series 4 (Elsevier, Amsterdam, 1991)
51. A.L. Highsmith, K.L. Reifsneider, Stiffness Reduction Mechanisms, in *Composite Laminates, Damage in Composite Materials, ASTM STP 775*, ed. by K.L. Reifsneider (American Society for Testing and Materials, West Conshohocken, PA, 1982), pp. 103–117

52. R. Talreja, *Fatigue of Composite Materials* (Technomic, Lancaster Pennsylvania, 1987)
53. S.I. Andersen, P. Brondsted, H. Lilholt, Fatigue of polymeric composites for wingblades and the establishment of stiffness-controlled fatigue diagrams. in *Proceedings of 1996 European Union Wind Energy Conference*, Göteborg, Sweden, (20–24 May 1996) pp. 950–953
54. W. Van Paepegem, Fatigue damage modeling of composite materials with the phenomenological residual stiffness approach, in *Fatigue Life Prediction of Composites and Composite Structures*, ed. by A.P. Vassilopoulos (Woodhead Publishing Ltd., Cambridge, 2010)
55. W. Hwang, K.S. Han, Fatigue of composites-fatigue modulus concept and life prediction. J. Compos. Mater. **20**(2), 154–165 (1986)
56. H.T. Hahn, R.Y. Kim, Fatigue behavior of composite laminate. J. Compos. Mater. **10**(2), 156–180 (1976)
57. J.A.M. Ferreira, P.N. Reis, J.D.M. Costa, M.O.W. Richardson, Fatigue behavior of composite adhesive lap joints. Compos. Sci. Technol. **62**(10–11), 1373–1379 (2002)
58. T. Keller, A. Zhou, Fatigue behavior of adhesively bonded joints composed of pultruded GFRP adherends for civil infrastructure applications. Compos Part A-Appl S **37**(8), 1119–1130 (2006)
59. Y. Zhang, A.P. Vassilopoulos, T. Keller, Stiffness degradation and fatigue life prediction of adhesively-bonded joints for fiber-reinforced polymer composites. Int. J. Fatigue **30**(10–11), 1813–1820 (2008)
60. M.J. Salkind, Fatigue of composites, in *Composite Materials, Testing And Design, ASTM STP 497*, ed. by H.T. Corten (American Society for Testing and Materials, West Conshohocken, PA, 1972), pp. 143–169
61. T.P. Philippidis, A.P. Vassilopoulos, Fatigue design allowables for GFRP laminates based on stiffness degradation measurements. Compos. Sci. Technol. **60**(15), 2819–2828 (2000)
62. T.P. Philippidis, A.P. Vassilopoulos, Fatigue of composite laminates under off-axis loading. Int. J. Fat. **21**, 253–262 (1999)
63. Anon. IEC-TC88-WG8 test guideline: "Full-scale structural testing of rotor blades for WTGS's", IEC 61400–23 (1998)